Author/s:
Zou, C;Manzie, C;Nesic, D

Title:
A Framework for Simplification of PDE-Based Lithium-Ion Battery Models

Date:
2016

Citation:
Zou, C., Manzie, C. & Nesic, D. (2016). A Framework for Simplification of PDE-Based Lithium-Ion Battery Models. IEEE Transactions on Control Systems Technology, 24 (5), pp.1594-1609. https://doi.org/10.1109/TCST.2015.2502899.

Persistent Link:
https://hdl.handle.net/11343/297872

A Framework for Simplification of PDE-Based Lithium-Ion Battery Models

Changfu Zou, *Student Member, IEEE*, Chris Manzie, *Senior Member, IEEE*, and Dragan Nešić, *Fellow, IEEE*

***Abstract*— Simplified models are commonly used in battery management and control, despite their (often implicit) limitations in capturing the dynamic behavior of the battery across a wide range of operating conditions. This paper seeks to develop a framework for battery model simplification starting from an initial high-order physics-based model that will explicitly detail the assumptions underpinning the development of simplified battery models. Starting from the basis of a model capturing the electrochemical, thermal, electrical, and aging dynamics in a set of partial differential equations, a systematic approach based on singular perturbations and averaging is used to simplify the dynamics through identification of disparate timescales inherent in the problem. As a result, libraries of simplified models with interconnections based on the specified assumptions are obtained. A quantitative comparison of the simplified models relative to the original model is used to justify the model reductions. To demonstrate the utility of the framework, a set of battery charging strategies is evaluated at reduced computational effort on simplified models.**

***Index Terms*— Averaging, battery models, charging strategy evaluation, lithium-ion (Li-ion) battery, model simplification, singular perturbation.**

I. Introduction

BATTERIES are widely used in applications ranging from portable electronic devices to automotive and smart electrical grids. Lithium-ion (Li-ion) batteries that exhibit high energy and power density along with no memory effect and low self-discharge relative to other cell chemistries like lead-acid and nickel–metal hydride batteries are the leading technology enabling further mobile electrification [1]. Common to all these applications is a desire to maintain battery lifetime without unduly sacrificing the performance of the battery. Battery models are used for evaluation of existing charging strategies, estimator and controller development, simulation, and optimization.

Manuscript received May 5, 2015; revised August 11, 2015 and October 29, 2015; accepted November 5, 2015. Manuscript received in final form November 14, 2015. This work was supported in part by the National Information and Communications Technology, Australia (NICTA), and in part by the Australian Research Council under Grant FT100100538. Recommended by Associate Editor C. Prieur.

C. Zou is with the Department of Mechanical Engineering, The University of Melbourne, Parkville, VIC 3010, Australia and NICTA Victoria, Australia (e-mail: cezou@student.unimelb.edu.au).

C. Manzie is with the Department of Mechanical Engineering, The University of Melbourne, Parkville, VIC 3010, Australia (e-mail: manziec@unimelb.edu.au).

D. Nešić is with the Department of Electrical and Electronic Engineering, The University of Melbourne, Parkville, VIC 3010, Australia (e-mail: dnesic@unimelb.edu.au).

Color versions of one or more of the figures in this paper are available online at http://ieeexplore.ieee.org.

Digital Object Identifier 10.1109/TCST.2015.2502899

The existing models currently used in most battery management systems are equivalent circuit models due to their low computational complexity. These models are essentially derived from empirical knowledge and experimental data in which the battery is idealized as an open-circuit voltage source connected with resistors, capacitors, and/or hysteresis voltage [2]–[4]. However, they are generally limited to low accuracy in predicting battery characteristics across a range of operating conditions, which leads to conservative utilization or excessive aging of the battery. In addition, the physical interpretation behind the system states and parameters is lost so that the models cannot provide insight into battery internal information such as the state of health (SOH). These shortcomings have spurred the development of physics-based battery models.

An electrochemistry-based model of a Li-ion cell was initially proposed in [5] based on porous electrode theory and concentrated solution theory. This pioneering work in modeling battery dynamics has been extensively reformulated [6]–[10]. Temperature plays an important role in battery management for both safety and optimal utilization, so it is necessary to include thermal dynamics. A general form of battery thermal models is developed in [11] to predict spatially distributed temperature variations. However, none of these papers have considered the dynamics of potentials and currents as they are fast time-varying states in a battery system. Furthermore, the dynamics of SOH are not covered by these models.

Since knowledge of SOH may be helpful in maintaining cell utility over the lifetime, considerable effort has been devoted to modeling battery degradation in the past decade. Empirical or semiempirical models derived by fitting experiment data [12] can capture SOH change at some conditions for a certain battery but are restricted by their system specific nature. An alternative approach in [13] and [14] proposed that the degradation process is proportional to the charge throughout a battery, and was shown to be accurate in predicting the calendar life or cycling life at low charging rates. To improve the range of model validity, Ramadass *et al.* [15] proposed a physics-based SOH model incorporating the growth of solid–electrolyte interface (SEI) film in the battery electrode, which is associated with capacity fade and active Li-ion consumption. The SEI film-based aging has been characterized as a dominant mechanism inducing electrochemical parasitic reaction [16]–[18], and the developed general model is widely employed in SOH simulation and control applications [19], [20].

Starting from the electrochemical model of [6], the thermal model of [11], and the SOH model of [15], a physics-based high-fidelity Li-ion battery model is proposed as the first contribution of this paper. This model captures the coupled electrochemical, thermal, electrical, and aging dynamics in a Li-ion battery system. The proposed battery model consists of a set of coupled nonlinear partial differential equations (PDEs) in multiple timescales. In view of this, model simplification is of significant importance for many real-world applications such as charging strategy evaluation, residual capacity and lifetime estimation, thermal management, cell balancing, and fast charging control. Partial simplifications were previously conducted on the temperature model [21] and the electrochemical model [22], [23]. To date, however, no rigorous simplification methodologies have been proposed for this high-fidelity battery model.

Singular perturbation theory for timescale separation of ordinary differential equation (ODE) systems has been well established [24]. However, for applications subject to singularly perturbed nonlinear systems in infinite dimensions, there are no available formal analysis tools, as far as we are aware. In other domains such as semiconductor optical amplifiers, where PDEs are necessary to describe the system models, a heuristic multiple-scale technique [25] is used to construct analytical solutions for the gain recovery dynamics, and the simulation results are shown to work well. To capture the spatially distributed nature but simplify the system complexity for feedback control applications, singular perturbation approaches have been used in thermal chemical vapor deposition reactor and crystal growth process through formulating PDEs in Hilbert space [26], [27]. Due to the proven efficacy in the previous work, similar approaches in the infinite dimensional Li-ion battery modeling problem may be applicable.

Consequently, the second contribution in this paper is the development of a model simplification framework for a Li-ion battery. The original PDE-based battery model is first reformulated in Hilbert space to precisely characterize its mathematical structure. Model simplification is systematically conducted using a singular perturbation approach and averaging theory. Families of battery models under different assumptions are thus obtained and associated with each other within a battery model simplification framework. This methodology for simplification of high-fidelity battery models is applicable to other battery types and models. The assumptions imposed on the system's physical and dynamic characteristics are quantitatively justified by simulation. The simplified models are not only well suited for analyzing the battery behavior but also beneficial for the development of model-based controllers and optimization algorithms.

The rest of this paper is organized as follows. In Section II, the full-order Li-ion battery model is described. Sections III and IV present our key contributions including the proposed model reformulation and model simplification framework. The derived simplified models are compared with the original model through simulations and implemented for assessing charging strategies in Sections V and VI separately. This is finally followed by the conclusion and future work in Section VII.

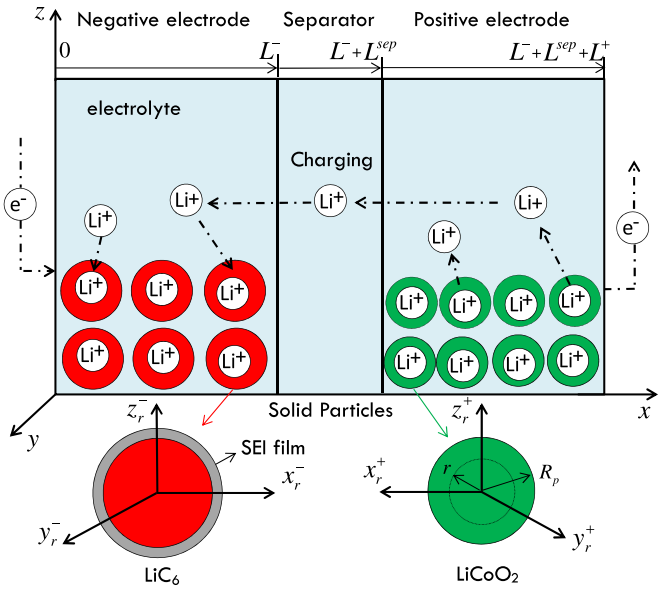

Fig. 1. Anatomy and schematic of a $LiCoO_2/LiC_6$ battery cell during the charging process (modified from [6]).

II. Full-Order Battery Model

In a Li-ion battery cell as provided in Fig. 1, the system dynamics represent the flow of Li-ions from the solid particles to the electrolyte along the radius direction r and from the positive electrode (cathode) to the negative electrode (anode) along the thickness direction x. Such Li-ion diffusion results in electrochemical, thermal, electrical, and aging phenomena associated with the main intercalation reaction and the side reaction.

In this section, a high-fidelity battery model that captures all these system dynamic characteristics is formulated. This initial model formulation will be a test bed measuring the accuracy and computational complexity for all later model simplifications. The interconnection of subsystems including the electrochemical (Σ^{ec}), thermal (Σ^T), electrical (Σ^e), and aging dynamics (Σ^{SOH}) is summarized in Fig. 2. In the rest of this section, each of these battery subsystems is elaborated using the notations in Table I.

A. Dynamics of Mass Diffusion

Under the battery potential difference, the Li-ions diffuse from the center to the surface of spherical solid particles where most of them undergo the main intercalation reaction, while a small part of them are involved in the side reaction that triggers battery degradation.

During the side reaction of a battery, a passive SEI film forms and grows leading to increased film resistance in the negative electrode, and this is accompanied by consumption of the active Li ions in the positive electrode [15]. Based on the mass conservation law applied to the Li-ion concentration, the lost number of Li ions per volume C^+_{loss} in the positive electrode is given by

$$C^+_{\text{loss}}(x,r,t) = \frac{Q_{\text{sr}}(x,t)}{Q_{\max}} \bar{C}^+_s(x,r,t) \tag{1}$$

TABLE I
NOMENCLATURE

A	Equivalent cross-sectional area of the battery cell	R_f	SEI film resistance
a	Interfacial area at the surface of solid particles	R_p	Radius of the solid particles
C_s	Li-ion concentration in solid particles	r	Distance along radius direction of solid particles
C_{ss}	Li-ion concentration at the surface of solid particles	T	Temperature
C_{loss}	Li-ion concentration lost	T_f	Temperature at the surface of battery cell
C_{smax}	Maximum possible solid-phase Li-ion concentration	U	Open circuit potential of the normal reaction
C_e	Li-ion concentration in the electrolyte	U_{sr}	Open circuit potential of the side reaction
c	Specific heat capacity	V	Terminal voltage
D_s^{eff}	Effective electric diffusion coefficient	x	Distance along battery thickness direction
D_e^{eff}	Effective ionic diffusion coefficient	α_n, α_p	Anodic/cathodic charge-transfer coefficient
F	Faraday's constant	α_{sr}	Charge-transfer coefficient of side reaction
h	Heat transfer coefficient between the cell and ambient	Δ_S	Entropy change
I	Applied current at terminal	η	Overpotential of the normal reaction
i_e	Local current in the electrolyte	η_{sr}	Overpotential of the side reaction
i_0	Exchange current density of the normal reaction	γ	Transference number of the anion
i_{0sr}	Exchange current density of the side reaction	κ^{eff}	Effective ionic conductivity in the electrolyte
J	Total Li-ion flux at the surface of solid particles	λ, δ_S	Heat conductivity/entropy change
J_I	Li-ion flux of the normal intercalation	μ_s	Volume fraction of solid particles in the electrode
J_{sr}	Li-ion flux of the side reaction	μ_e	Volume fraction of electrolyte in the electrode/separator
L	Total length of the battery cell	Φ_s	Electric potential in solid particles
L^-, L^+	The length of the negative/positive electrode	Φ_e	Electric potential in the electrolyte
M_f	Average molecular weight of SEI film	ρ	Mass density of battery cell
Q_{sr}	Capacity fade	ρ_f	Average density of SEI film
$Q_{\max}$	Maximum capacity of the battery	σ^{eff}	Effective electronic conductivity in the electrode
R	Universal gas constant	σ_f	Effective conductivity of SEI film
$-, +, sep$	Superscript denoting the negative electrode, positive electrode, and separator, respectively		

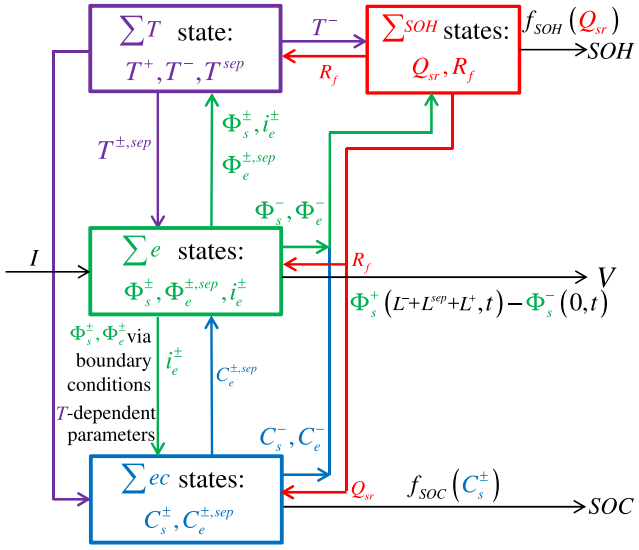

Fig. 2. Block diagram representation of a high-fidelity Li-ion battery model including the system input, outputs, state variables, and coupling relationships among the electrochemical, electrical, thermal, and aging subsystems.

where $\bar{C}_s$ is the ideal solid-phase Li-ion concentration in the absence of battery aging.

In the absence of battery aging, the mass transport in the solid particles can be described by Fick's law of diffusion and is given as [6], [28]

$$\frac{\partial \bar{C}_s^{\pm}(x,r,t)}{\partial t} = \frac{D_s^{\text{eff},\pm}}{r^2}\frac{\partial}{\partial r}\left(r^2\frac{\partial \bar{C}_s^{\pm}(x,r,t)}{\partial r}\right). \tag{2}$$

In the existing models of capacity fade, the initial cathode Li-ion concentration is updated in a discontinuous jump at the end of each charging operation to capture the aging effect. To describe the continuous interaction between Li-ion loss and capacity fade, the concentration dynamics in the positive electrode based on the concentration conservation property is proposed here as

$$\frac{\partial C_s^{+}(x,r,t)}{\partial t} = \frac{\partial \bar{C}_s^{+}(x,r,t)}{\partial t} - \frac{\partial C_{\text{loss}}^{+}(x,r,t)}{\partial t}. \tag{3}$$

The combination of (1)–(3) results in a dynamic equation simultaneously describing the Li-ion concentration diffusion and consumption

$$\frac{\partial C_s^{+}(x,r,t)}{\partial t} = \frac{\partial \bar{C}_s^{+}(x,r,t)}{\partial t} - \frac{Q_{\text{sr}}(x,t)}{Q_{\max}}\frac{\partial \bar{C}_s^{+}(x,r,t)}{\partial t} - \frac{\bar{C}_s^{+}(x,r,t)}{Q_{\max}}\frac{\partial Q_{\text{sr}}(x,t)}{\partial t} \tag{4}$$

where the first term of the right-hand side of (4) represents the normal Li-ion diffusion, and the last two terms denote the Li-ion loss caused by battery side reaction.

Inside the negative electrode, the active Li-ion loss is typically ignored [15], [16], allowing the state behavior of Li-ion concentration to be presented as (2), namely

$$\frac{\partial C_s^{-}(x,r,t)}{\partial t} = \frac{D_s^{\text{eff},-}}{r^2}\frac{\partial}{\partial r}\left(r^2\frac{\partial C_s^{-}(x,r,t)}{\partial r}\right). \tag{5}$$

In the electrolyte, the change of Li-ion concentration is related to its gradient-induced diffusive flow and the local electrolyte current and is governed by [5], [6]

$$\frac{\partial C_e^{j}(x,t)}{\partial t} = \frac{\partial}{\partial x}\left(\frac{D_e^{\text{eff},j}}{\mu_e^{j}}\frac{\partial C_e^{j}(x,t)}{\partial x}\right) + \frac{\gamma^{j}}{F\mu_e^{j}}\frac{\partial i_e^{j}}{\partial x} \tag{6}$$

where $j \in \{+, -, \text{sep}\}$.

B. Dynamics of Electrical States

The signal transmission of local potentials and currents in the solid particles and the electrolyte is very fast. Their steady-state behaviors can be modeled by applying Ohm's law, modified Ohm's law, and the law of charge conservation, respectively, as provided in [6]. Here, the dynamic equations that explicitly describe the transient behavior of the state variables of potentials and currents are proposed in the following:

$$\epsilon_{\Phi s}\frac{\partial \Phi_s^{\pm}(x,t)}{\partial t} = \frac{\partial \Phi_s^{\pm}(x,t)}{\partial x} + \frac{I(t)-i_e^{\pm}(x,t)}{\sigma^{\text{eff},\pm}} \tag{7}$$

$$\epsilon_{\Phi e}\frac{\partial \Phi_e^{j}(x,t)}{\partial t} = \frac{\partial \Phi_e^{j}(x,t)}{\partial x} + \frac{i_e^{j}(x,t)}{\kappa^{\text{eff},j}} - \frac{2R\gamma^{j}T^{j}(x,t)}{F}\frac{\partial \ln C_e^{j}(x,t)}{\partial x} \tag{8}$$

$$\epsilon_{ie}\frac{\partial i_e^{\pm}(x,t)}{\partial t} = \frac{\partial i_e^{\pm}(x,t)}{\partial x} - Fa^{\pm}J^{\pm}(x,t) \tag{9}$$

where $\epsilon_{\Phi s}$, $\epsilon_{\Phi e}$, and ϵ_{ie} are small positive parameters and their reciprocals are, respectively, related to the transmission speeds of electric potential, ionic potential, and electrolyte current.

Based on Kirchoff's current law applied in the x-direction, the input current through the cross section of a cell is uniform, so that the local solid-phase and electrolyte currents satisfy

$$i_s(x,t) + i_e(x,t) = I(t). \tag{10}$$

The total Li-ion flux J consists of the normal intercalation reaction flux J_I and side reaction flux J_{sr}. J_I is governed by the Butler–Volmer kinetic equation and can be expressed as a function of $\Phi_s, \Phi_e, C_s, C_e, T$, and R_f [29]

$$J_I^{\pm}(x,t) = \frac{i_0^{\pm}(x,t)}{F}\left(e^{\frac{\alpha_n F\eta^{\pm}(x,t)}{RT^{\pm}(x,t)}} - e^{-\frac{\alpha_p F\eta^{\pm}(x,t)}{RT^{\pm}(x,t)}}\right) \tag{11}$$

where the exchange current density i_0 and the overpotential η are described as

$$i_0^{\pm}(x,t) = k^{\pm}C_e^{\pm}(x,t)^{\alpha_n}\left(C_{\text{smax}}^{\pm} - C_{\text{ss}}^{\pm}(x,t)\right)^{\alpha_n}C_{\text{ss}}^{\pm}(x,t)^{\alpha_p}$$

$$\eta^{\pm}(x,t) = \Phi_s^{\pm}(x,t) - \Phi_e^{\pm}(x,t) - U^{\pm}(x,t) - FR_f(x,t)J^{\pm}(x,t).$$

Here, k is the reaction rate constant and C_{ss} is the Li-ion concentration at the surface of these particles

$$C_{\text{ss}}^{\pm}(x,t) := C_s^{\pm}\left(x, r = R_p^{\pm}, t\right). \tag{12}$$

The open-circuit potential U can be evaluated as a nonlinear function of the surface Li-ion concentration [8], [28].

C. Thermal Dynamics

The heat sources inside a cell include the reaction heat generation, reversible heat generation, and ohmic heat generation. The generated heat is transported through the battery internal conductivity and convection between the battery surface and the surrounding environment. To capture temperature distribution and evolution in a Li-ion battery cell, the thermal balance equation is provided as [11]

$$\rho^{j}c^{j}\frac{\partial T^{j}(x,t)}{\partial t} = \lambda^{j}\frac{\partial^2 T^{j}(x,t)}{\partial x^2} - \left(I(t) - i_e^{j}(x,t)\right)\frac{\partial \Phi_s^{j}(x,t)}{\partial x} - i_e^{j}(x,t)\frac{\partial \Phi_e^{j}(x,t)}{\partial x} + Fa^{j}J^{j}(x,t)\eta^{j}(x,t) + Fa^{j}J^{j}(x,t)T^{j}(x,t)\Delta_S^{j}. \tag{13}$$

On the right-hand side of (13), the second and third terms represent the reaction heat, and the last two terms are separately the ohmic heat and reversible heat. From the above equation, it follows that the electrical states Φ_s, Φ_e, and i_e are directly involved in heat generation. The elevated temperature in turn affects the main intercalation reaction through (8) and accelerates the dynamics of battery aging via (16).

D. Dynamics of Battery Aging

The main terminal product resulting from side reaction is a resistive and insoluble SEI film that forms in the graphite anode [15], [16]. As battery operating cycles increase, such a film grows and leads to successive capacity fade and internal resistance rise.

A lumped capacity fade has been formulated in the initial SOH model of [15]. However, physically, the side reaction as well as its resulting parasitic flux and SEI film may exhibit strong spatial variations. To model this process accurately, a spatially distributed aged capacity $Q_{\text{sr}}(x,t)$ is considered in establishing the full-order battery model. With this in mind, the dynamic equations of capacity fade and internal resistance are proposed in the following form:

$$\frac{\partial Q_{\text{sr}}(x,t)}{\partial t} = -Fa^{-}A^{-}L^{-}J_{\text{sr}}(x,t) \tag{14}$$

$$\frac{\partial R_f(x,t)}{\partial t} = -\frac{M_f}{\rho_f\sigma_f}J_{\text{sr}}(x,t). \tag{15}$$

In (14) and (15), by assuming the side reaction to be irreversible, the side reaction flux J_{sr} can be modeled by the Tafel equation [15], [29]

$$J_{\text{sr}}(x,t) = \frac{-i_{0\text{sr}}}{F}e^{\frac{-F\alpha_{\text{sr}}\eta_{\text{sr}}(x,t)}{RT^{-}(x,t)}} \tag{16}$$

where the overpotential that determines the rate of side reaction is provided by

$$\eta_{\text{sr}}(x,t) = \Phi_s^{-}(x,t) - \Phi_e^{-}(x,t) - U_{\text{sr}} - FR_f(x,t)J^{-}(x,t).$$

E. Boundary Conditions

The complete battery cell over the negative electrode, separator, and positive electrode is linked through the SEIs and the electrode–separator interfaces. At the center of the solid particles, where $r = 0$, the Li-ion diffusion rate is zero due to symmetry of spherical diffusion. While, at the surface of solid particles, where $r = R_p$, the Li-ion concentration flux is governed by the diffusion rate between the solid particles and electrolyte. At the current collectors, namely, $x = 0$ and $x = L$, the electrolyte currents and the electrolyte diffusion rates are all zero, and the thermal transport is determined by Newton's cooling law. At the electrode–separator

interfaces, where $x = L^-$ and $x = L^- + L^{\text{sep}}$, the electrolyte concentration and temperature are continuous and preserve mass and energy conservation properties. Particularly, in the separator, there is no solid particle as well as solid-phase Li-ions so that for their governing equations, $C_s = \Phi_s = Q_{\text{sr}} = R_f = 0$ and $i_e(x,t) = I(t)$.

F. System Outputs

The system outputs of interest are the terminal voltage $V(t)$, state of charge (SOC), and SOH. The terminal voltage is presented as the difference between the positive and negative electrical potentials at the terminals, and is a measurable output. The SOC in each electrode is defined as the ratio between the averaged available Li-ion concentration and maximum possible concentration [6]. SOC represents the averaged available charge contained in active materials and is used to evaluate the energy left in the battery. SOH is quantitatively evaluated by the average capacity fade in the anode electrode and the initial maximum available capacity [18]. With this in mind, these system outputs are formulated as follows:

$$V(t) = \Phi_s^+(L,t) - \Phi_s^-(0,t) \tag{17}$$

$$\text{SOC}^{\pm}(t) = \frac{3}{L^{\pm}R_p^{3,\pm}} \int_0^{L^{\pm}} \int_0^{R_p^{\pm}} \frac{C_s^{\pm}(x,r,t)}{C_{\text{smax}}^{\pm}} dr dx \tag{18}$$

$$\text{SOH}(t) = 1 - \int_0^{L^-} \frac{Q_{\text{sr}}(x,t)}{Q_{\max}} dx. \tag{19}$$

It is worth mentioning that the outputs in (17)–(19) are finite dimensional, whereas the states are all infinite dimensional.

G. Summary of the Battery Model

To sum up, the initial high-fidelity battery system (referred to as Σ) is composed of four subsystems that, respectively, describe the electrochemical, thermal, electrical, and aging phenomena. The dynamic characteristics are represented by (4)–(16), leading to a set of 17 coupled nonlinear PDEs over two spatial dimensions. Besides incorporating all these relevant system dynamics and their coupling relationships into an individual model, three modifications have been proposed. First, the continuous coupling effects between the normal electrochemical reaction and the side reaction with respect to the solid-phase Li-ion concentration have been captured, as provided in (4). The dynamic equations of potentials and currents rather than their steady states are explicitly formulated in (7)–(9). In addition, the spatially distributed capacity fade has been introduced in (14) to reflect the physical nature of battery degradation.

III. Model Reformulation in Hilbert Space

In this section, the full-order battery model is reformulated in Hilbert space in order to precisely characterize its mathematical structure and to uncover the singular perturbation structure underlying this model. The key idea is to present the PDE system in an operator differential equation form using function mappings between the Euclidean space and the Hilbert space.

To do so, the common features of the battery dynamic equations are first extracted. Define the state variables as a vector $\bar{\mathbf{x}} := [\bar{\mathbf{x}}^-, \bar{\mathbf{x}}^+, \bar{\mathbf{x}}^{\text{sep}}]^T$, where in the negative electrode $\bar{\mathbf{x}}^- := [C_s^-, C_e^-, \Phi_s^-, \Phi_e^-, i_e^-, T^-, Q_{\text{sr}}, R_f]^T$, in the separator $\bar{\mathbf{x}}^{\text{sep}} := [C_e^{\text{sep}}, \Phi_e^{\text{sep}}, T^{\text{sep}}]^T$, and in the positive electrode $\bar{\mathbf{x}}^+ := [C_s^+, C_e^+, \Phi_s^+, \Phi_e^+, i_e^+, T^+]^T$. The system input u is defined as $u := I(t)$. The domain of definition for all the state variables is $\mathcal{D}(x,r) = \{(x,r) | x \in [0,L], r \in [0,R_p]\}$. $\mathbf{y}_c$ and $\mathbf{y}_m$ separately denote the unmeasurable outputs and the measured output with $g(\cdot)$ being a column vector function defined as $\mathbf{y}_c := [\text{SOC}^-(t), \text{SOC}^+(t), \text{SOH}(t)]^T$ and $\mathbf{y}_m := V(t)$.

Then the PDE-based battery system Σ may be rewritten in the general form

$$\frac{\partial \bar{\mathbf{x}}}{\partial t} = F_1 \frac{\partial \bar{\mathbf{x}}}{\partial r} + S_1 \frac{\partial \bar{\mathbf{x}}}{\partial x} + F_2 \frac{\partial^2 \bar{\mathbf{x}}}{\partial r^2} + S_2 \frac{\partial^2 \bar{\mathbf{x}}}{\partial x^2} + H(\bar{\mathbf{x}}, u) \tag{20}$$

$$\mathbf{y}_c = g(\bar{\mathbf{x}}) \tag{21}$$

$$\mathbf{y}_m = q(\bar{\mathbf{x}}) \tag{22}$$

subject to the boundary conditions

$$\begin{aligned}
C_1 \bar{\mathbf{x}}^-|_{x=0} &= 0, \quad C_3 \bar{\mathbf{x}}^+|_{x=L} = 0 \\
C_2 \frac{\partial \bar{\mathbf{x}}^-}{\partial x}\bigg|_{x=0} &= D_1, \quad C_4 \frac{\partial \bar{\mathbf{x}}^+}{\partial x}\bigg|_{x=L} = D_2 \\
C_5 \frac{\partial \bar{\mathbf{x}}^-}{\partial r}\bigg|_{r=0} &= 0, \quad C_6 \frac{\partial \bar{\mathbf{x}}^+}{\partial r}\bigg|_{r=0} = 0 \\
C_7 \frac{\partial \bar{\mathbf{x}}^-}{\partial r}\bigg|_{r=R_p^-} &= D_3, \quad C_8 \frac{\partial \bar{\mathbf{x}}^+}{\partial r}\bigg|_{r=R_p^+} = D_4 \\
\bar{\mathbf{x}}^-|_{x=L^-} &= D_5 \bar{\mathbf{x}}^{\text{sep}}|_{x=L^-} \\
\frac{\partial \bar{\mathbf{x}}^-}{\partial x}\bigg|_{x=L^-} &= D_6 \frac{\partial \bar{\mathbf{x}}^{\text{sep}}}{\partial x}\bigg|_{x=L^-} \\
\bar{\mathbf{x}}^{\text{sep}}|_{x=L^-+L^{\text{sep}}} &= D_7 \bar{\mathbf{x}}^+|_{x=L^-+L^{\text{sep}}} \\
\frac{\partial \bar{\mathbf{x}}^{\text{sep}}}{\partial x}\bigg|_{x=L^-+L^{\text{sep}}} &= D_8 \frac{\partial \bar{\mathbf{x}}^+}{\partial x}\bigg|_{x=L^-+L^{\text{sep}}}.
\end{aligned} \tag{23}$$

The initial conditions are given by

$$\bar{\mathbf{x}}(t = t_0, x, r) = \bar{\mathbf{x}}_0. \tag{24}$$

In (20), F_1, F_2, S_1, S_2, and H are all matrix functions and can be derived from the battery dynamic equations (4)–(16). In (23), $C_1, \ldots, C_8$ and $D_1, \ldots, D_8$ are parameter matrices. The explicit forms of all these functions and parameter matrices are provided in the Appendix.

To present the PDE system precisely and also simplify the notation, the infinite-dimensional system (20)–(22) is reformulated within the Hilbert space $\mathscr{H}(\mathcal{D}, \mathbb{R}^n)$. It is a space of n-D vector functions defined on a spatial interval and being square integrable [27]. Define the state function $\mathbf{x}$ on $\mathscr{H}$ as

$$\mathbf{x}(t) = \bar{\mathbf{x}}(x,r,t) \quad \forall t > 0 \quad \forall (x,r) \in \mathcal{D}(x,r)$$

the operator $\mathcal{F}$ in $\mathscr{H}(\mathcal{D}, \mathbb{R}^n)$ as

$$\begin{aligned}
\mathcal{F}\mathbf{x} &= F_1 \frac{\partial \bar{\mathbf{x}}}{\partial r} + S_1 \frac{\partial \bar{\mathbf{x}}}{\partial x} + F_2 \frac{\partial^2 \bar{\mathbf{x}}}{\partial r^2} + S_2 \frac{\partial^2 \bar{\mathbf{x}}}{\partial x^2} \\
\mathbf{x} \in D(\mathcal{F}) &= \{\mathbf{x} \in \mathscr{H}(\mathcal{D}, \mathbb{R}^n);\ \text{Eqs: (23)}\}
\end{aligned}$$

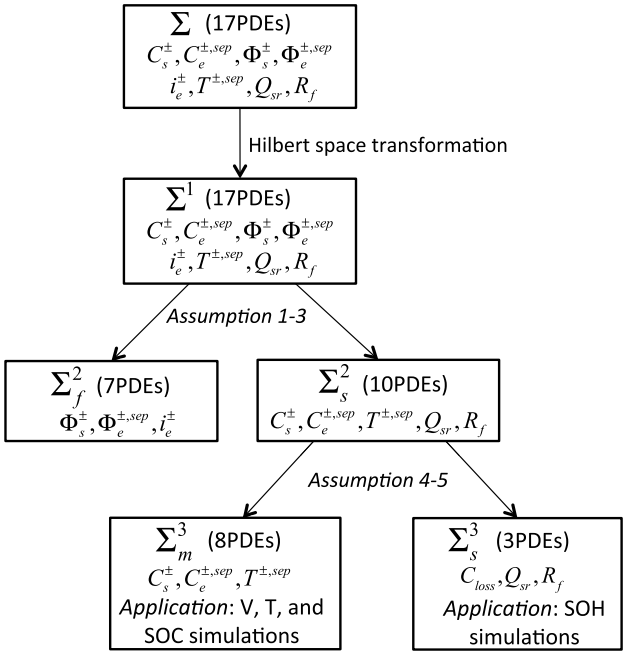

Fig. 3. Flowchart to elucidate the procedure of battery model simplification.

and the output operators as

$$\mathcal{G}\mathbf{x} = g, \quad \mathcal{Q}\mathbf{x} = q.$$

Then, the battery system (20)–(24) may be represented compactly in the form

$$\begin{aligned} \Sigma^1 : \ \dot{\mathbf{x}} &= \mathcal{F}\mathbf{x} + H(\mathbf{x}, u), \quad \mathbf{x}(0) = \mathbf{x}_0 \\ \mathbf{y}_c &= \mathcal{G}\mathbf{x} \\ \mathbf{y}_m &= \mathcal{Q}\mathbf{x} \end{aligned} \tag{25}$$

where $H(\mathbf{x}(t), u(t)) = H(\bar{\mathbf{x}}(x, r, t), u(t))$ and $\mathbf{x}_0 = \bar{\mathbf{x}}_0$.

IV. Model Simplification Procedure

The initial physics-based model presented in the previous section is capable of capturing battery system dynamics but is generally too complex for most model-based applications. In the following, we use a systematic procedure to develop a battery modeling framework. Assumptions imposed on battery physical and chemical properties are gradually introduced, justified, and remarked.

The modeling complexity is predominantly attributed to the mathematical representation of nonlinear PDEs and coupled electrical dynamics, mass and thermal diffusion, and battery aging in different timescales associated with oscillated trajectories. With this in mind, model simplifications are systematically executed and the exact sequence is schematically interpreted in Fig. 3. First, by the application of a singular perturbation approach, the fast states are eliminated to derive a simplified (reduced) model Σ_s^2. In the sequel, based on Σ_s^2, a singular perturbation approach and averaging theory are appropriately combined to decouple the medium and slow timescale variables. As a consequence, a boundary layer system Σ_m^3 and a reduced system Σ_s^3 are obtained.

A. Theory for Model Simplification 1: Models Σ_f^2 and Σ_s^2

In the first stage, model simplification is motivated by insight into the battery dynamics. The electrical dynamics are much faster than the mass and thermal diffusion process. The difference in the magnitudes stems from the small parameters $\epsilon_{\Phi s}, \epsilon_{\Phi e}$, and ϵ_{ie} in (7)–(9). Based on the physical meaning of them, these parameters are assumed to have the same magnitude without loss of generality. Define $\epsilon_1 := \epsilon_{\Phi s} = \epsilon_{\Phi e} = \epsilon_{ie}$, where ϵ_1 is a small positive parameter. To investigate the timescale separation, the system (25) can be written in the standard form of singularly perturbed systems

$$\begin{aligned} \Sigma^1 : \ \dot{\mathbf{x}}_s &= \mathcal{F}_s\mathbf{x}_s + H_s(\mathbf{x}_s, \mathbf{x}_f, u), \mathbf{x}_s(0) = \mathbf{x}_{s0} \\ \epsilon_1\dot{\mathbf{x}}_f &= \mathcal{F}_f\mathbf{x}_f + H_f(\mathbf{x}_s, \mathbf{x}_f, u), \mathbf{x}_f(0) = \mathbf{x}_{f0} \\ \mathbf{y}_c &= \mathcal{G}[\mathbf{x}_s, \mathbf{x}_f]^T \\ \mathbf{y}_m &= \mathcal{Q}[\mathbf{x}_s, \mathbf{x}_f]^T \end{aligned} \tag{26}$$

where in the negative electrode, the state function $\mathbf{x}$ can be expressed more explicitly to include $\mathbf{x}_s^- := [C_s^-, C_e^-, T^-, Q_{\rm sr}, R_f]^T$ and $\mathbf{x}_f^- := [\Phi_s^-, \Phi_e^-, i_e^-]^T$. Similar cases can be done for the positive electrode and the separator. The functions H_s and H_f are continuous and bounded in their arguments for $(\mathbf{x}_s, \mathbf{x}_f, u) \in \mathscr{H}_s \times \mathscr{H}_f \times \mathbb{U}$, where $\mathscr{H}_s$ and $\mathscr{H}_f$ are subspaces of $\mathscr{H}$.

Assumption 1: Within battery operating processes, the parameter ϵ_1 involved in electrical dynamics satisfies $\epsilon_1 \ll 1$.

Justification for Assumption 1: Typically, a charge or discharge operation associated with the diffusion process and the chemical reaction is completed within several minutes or hours. Meanwhile, the signal transmission speeds of potentials and currents are very large quantities leading to time constants of microseconds order [30]. Thus, in comparison with the electrochemical and thermal states, which are nominally of order 1 in Σ^1, the dynamics of potentials and currents result in a sufficiently small ϵ_1.

Remark 1: With the parameter ϵ_1 justified to be sufficiently small, the model structure of (26) guides the use of singular perturbation approaches for model simplification of the battery system. Christofides [26] has some results using a singular perturbation approach on other classes of PDE systems. And a similar approach was pursued in [25] for photonics applications. However, without rigorous theoretical justification, this work will investigate the validity of singular perturbation techniques via simulations.

Assumption 2: In the timescale τ measured from the fast electrical dynamics, the variation of the input current u is sufficiently slow.

Justification for Assumption 2: For practical utilization of Li-ion batteries, due to physical limitation of battery chargers or power converters, the operating current typically changes in a time period of seconds or longer. Compared with the fast dynamics, the change of u is negligibly slow so that it can be considered as a constant in the fast timescale.

Based on Assumption 1, ϵ_1 is set to zero, leading to a fundamental and abrupt change in the dynamic properties of the fast state $\mathbf{x}_f$. The differential equation of $\mathbf{x}_f$ in (26) is

replaced by an algebraic equation

$$0 = \mathcal{F}_f \mathbf{x}_f + H_f(\mathbf{x}_s, \mathbf{x}_f, u). \tag{27}$$

The real root of (27) is known to exist in the arguments $\forall t > 0$ and $\forall (x, r) \in \mathcal{D}(x, r)$ and is derived as $\mathbf{x}_f^* = h(\mathbf{x}_s, u)$.

As a result, the fast dynamics for $\mathbf{x}_f$ are excluded from the original battery system and instead its quasi-steady state $h(\mathbf{x}_s, u)$ is considered. The full-order model Σ^1 is simplified to the slow (reduced) model with respect to the slow states $\mathbf{x}_s$ and is further presented as

$$\begin{aligned} \Sigma_s^2: \quad \dot{\mathbf{x}}_s &= \mathcal{F}_s \mathbf{x}_s + H_s(\mathbf{x}_s, h(\mathbf{x}_s, u), u), \quad \mathbf{x}_s(0) = \mathbf{x}_{s0} \\ \mathbf{y}_c &= \mathcal{G}[\mathbf{x}_s, h(\mathbf{x}_s, u)]^T \\ \mathbf{y}_m &= \mathcal{Q}[\mathbf{x}_s, h(\mathbf{x}_s, u)]^T. \end{aligned} \tag{28}$$

Remark 2: The slow model (28) with lumped battery degradation and without consideration of temperature dynamics is typically used as a starting point for model order reduction in [19] and [23]. A complete battery model is considered in this paper and demonstrates the use of a singular perturbation approach for PDE-based battery model simplification. The underlying assumption imposed on the simplified model is explicitly stated and justified.

Having established the reduced battery system, we now investigate the boundary layer system regarding to the state variables $\mathbf{x}_f$. In the fast timescale $\tau := (t - t_0)/\epsilon_1$, the battery model of (26) is readily modified to

$$\frac{d\mathbf{x}_s}{d\tau} = \epsilon_1 \mathcal{F}_s \mathbf{x}_f + \epsilon_1 H_s(\mathbf{x}_s, \mathbf{x}_f, u) \tag{29}$$

$$\frac{d\mathbf{x}_f}{d\tau} = \mathcal{F}_f \mathbf{x}_f + H_f(\mathbf{x}_s, \mathbf{x}_f, u). \tag{30}$$

By setting $\epsilon_1 = 0$, the differential equation (29) is degenerated into

$$\frac{d\mathbf{x}_s}{d\tau} = 0 \Rightarrow \mathbf{x}_s(\tau) = \mathbf{x}_{s0}. \tag{31}$$

Through (31), the dynamics of the slow state $\mathbf{x}_s$ are eliminated by freezing its value on $\mathbf{x}_{s0}$. This allows the battery model Σ^1 to be described by less state variables as well as less governing PDEs.

Based on Assumptions 1 and 2, there exists $u(t) = u(t_0 + \epsilon_1 \tau) \approx u(t_0)$. In view of this, the boundary layer method [31] can be applied here to investigate the fast dynamics individually in the battery system. Combining this and (30), the fast state $\mathbf{x}_f$ can be therefore decoupled from the original model and results in the following boundary layer (fast) system:

$$\Sigma_f^2: \quad \frac{d\mathbf{x}_f}{d\tau} = \mathcal{F}_f \mathbf{x}_f + H_f(\mathbf{x}_{s0}, \mathbf{x}_f, u_0), \quad \mathbf{x}_f(0) = \mathbf{x}_{f0}. \tag{32}$$

To shift the quasi-steady state of $\mathbf{x}_f$ to the origin, we define $\mathbf{z}_f = \mathbf{x}_f - h(\mathbf{x}_{s0}, u_0)$ and (32) can be reformulated as

$$\begin{aligned} \frac{d\mathbf{z}_f}{d\tau} &= \mathcal{F}_f(\mathbf{z}_f + h(\mathbf{x}_{s0}, u_0)) \\ &\quad + H_f(\mathbf{x}_{s0}, \mathbf{z}_f + h(\mathbf{x}_{s0}, u_0), u_0). \end{aligned} \tag{33}$$

Assumption 3: The boundary layer battery system given in (33) is uniformly globally exponentially stable.

Justification for Assumption 3: As there is no established theory to analytically justify this assumption, it will be tested numerically in Section V.

Remark 3: Assumption 3 for the boundary layer system has the similar structure with the classical singular perturbation theory of [24]. When this assumption holds, the trajectories of the fast state variables $\mathbf{x}_f$ in the original battery model Σ^1 will exponentially converge to its quasi-steady state governed by (27).

In this section, the electrical phenomenon and electrochemical-thermal-aging phenomenon have been identified to exhibit two timescales. A systematic procedure for developing simplified models with interconnections based on clearly specified assumptions has been proposed.

B. Application to Battery Models: Stage I

With simplified models obtained using a singular perturbation approach in Section IV-A, these theoretical results are applied to the Li-ion battery system.

The reduced battery system Σ_s^2 containing electrochemical, thermal, and aging dynamics is explicitly provided with battery states and parameters

$$\begin{aligned} \frac{\partial \bar{C}_s^+(x,r,t)}{\partial t} &= \frac{D_s^{\text{eff},+}}{r^2} \frac{\partial}{\partial r}\left(r^2 \frac{\partial \bar{C}_s^+(x,r,t)}{\partial r}\right) \\ \frac{\partial C_s^+(x,r,t)}{\partial t} &= \frac{\partial \bar{C}_s^+(x,r,t)}{\partial t} - \frac{Q_{\text{sr}}(x,t)}{Q_{\max}} \frac{\partial \bar{C}_s^+(x,r,t)}{\partial t} \\ &\quad - \frac{\bar{C}_s^+(x,r,t)}{Q_{\max}} \frac{\partial Q_{\text{sr}}(x,t)}{\partial t} \\ \frac{\partial C_s^-(x,r,t)}{\partial t} &= \frac{D_s^{\text{eff},-}}{r^2} \frac{\partial}{\partial r}\left(r^2 \frac{\partial C_s^-(x,r,t)}{\partial r}\right) \\ \frac{\partial C_e^j(x,t)}{\partial t} &= \frac{\partial}{\partial x}\left(\frac{D_e^{\text{eff},j}}{\mu_e^j} \frac{\partial C_e^j(x,t)}{\partial x}\right) + \frac{\gamma^j}{F\mu_e^j} \frac{\partial i_e^j}{\partial x} \\ \rho^j c^j \frac{\partial T^j(x,t)}{\partial t} &= \lambda^j \frac{\partial^2 T^j(x,t)}{\partial x^2} - \big(I(t) - i_e^j(x,t)\big) \frac{\partial \Phi_s^j(x,t)}{\partial x} \\ &\quad - i_e^j(x,t) \frac{\partial \Phi_e^j(x,t)}{\partial x} + F a^j J^j(x,t) \eta^j(x,t) \\ &\quad + F a^j J^j(x,t) T^j(x,t) \Delta_S^j \\ \frac{\partial Q_{\text{sr}}(x,t)}{\partial t} &= -F a^- A^- L^- J_{\text{sr}}(x,t) \\ \frac{\partial R_f(x,t)}{\partial t} &= -\frac{M_f}{\rho_f \sigma_f} J_{\text{sr}}(x,t). \end{aligned}$$

In the above equations, the fast electrical state variables, namely, $\Phi_s^{\pm}$, Φ_e^j, and $i_e^{\pm}$, converge to their quasi-steady states instantaneously and are governed by

$$\begin{aligned} \frac{\partial \Phi_s^{\pm}(x,t)}{\partial x} &= -\frac{I(t) - i_e^{\pm}(x,t)}{\sigma^{\pm}} \\ \frac{\partial \Phi_e^j(x,t)}{\partial x} &= -\frac{i_e^j(x,t)}{\kappa^j} + \frac{2R\gamma^j T^j}{F} \frac{\partial \ln C_e^j(x,t)}{\partial x} \\ \frac{\partial i_e^{\pm}(x,t)}{\partial x} &= F a^{\pm} J^{\pm}(x,t). \end{aligned}$$

To reflect the result of model simplification in (32) explicitly, the fast battery system Σ_f^2 representing the

electrical dynamics is further obtained in the following:

$$\frac{\partial \Phi_s^{\pm}(x,t)}{\partial \tau} = \frac{\partial \Phi_s^{\pm}(x,t)}{\partial x} + \frac{I_0 - i_e^{\pm}(x,t)}{\sigma^{\pm}}$$
$$\frac{\partial \Phi_e^{j}(x,t)}{\partial \tau} = \frac{\partial \Phi_e^{j}(x,t)}{\partial x} + \frac{i_e^{j}(x,t)}{\kappa^{j}}$$
$$\frac{\partial i_e^{\pm}(x,t)}{\partial \tau} = \frac{\partial i_e^{\pm}(x,t)}{\partial x} - Fa^{\pm}J^{\pm}(x,t)$$

where

$$J^{\pm}(x,t) = \frac{i_0^{\pm}}{F}\left(e^{\frac{\alpha_n F \eta^{\pm}(x,t)}{RT_0}} - e^{-\frac{\alpha_p F \eta^{\pm}(x,t)}{RT_0}}\right)$$
$$i_0^{\pm} = k^{\pm} C_{e0}{}^{\alpha_n} \left(C_{\text{smax}}^{\pm} - C_{s0}^{\pm}\right)^{\alpha_n} C_{s0}^{\pm\,\alpha_p}$$
$$\eta^{\pm}(x,t) = \Phi_s^{\pm}(x,t) - \Phi_e^{\pm}(x,t) - U^{\pm}\left(C_{s0}^{\pm}\right) - FR_{f0}J^{\pm}(x,t).$$

Here, the system input current I and the state variables $C_s^{\pm}$, C_e^j, T^j, Q_{sr}, and R_f are all set to their initial values.

C. Theory for Model Simplification 2: Models Σ_m^3 and Σ_s^3

Possible model simplification is further investigated in this section for the battery model Σ_s^2. The normal intercalation reaction and side reaction simultaneously occur during battery operation. However, the normal diffusion involved in mass and thermal phenomena is much faster than the aging progress that is typically quantified on the magnitude of months or years. This difference is essentially attributed by the normal intercalation reaction flux and side reaction flux where $J_I \gg J_{\text{sr}}$. Studies on (11) and (16) further show that $i_0 \gg i_{0\text{sr}}$, in which $i_{0\text{sr}}$ is a positive parameter on the order of $1e-6$, and in contrast, the value of i_0 is as large as 1 [15]. With this in mind, define $\epsilon_2 := i_{0\text{sr}}$, then the system of (26) is rewritten as

$$\begin{aligned}
\dot{\mathbf{x}}_{s'} &= \epsilon_2 \mathcal{F}_{s'}\mathbf{x}_{s'} + \epsilon_2 H_{s'}(\mathbf{x}_{s'}, \mathbf{x}_m, h(\mathbf{x}_{s'}, \mathbf{x}_m, u), u)\\
\mathbf{x}_{s'}(0) &= \mathbf{x}_{s'0}\\
\dot{\mathbf{x}}_m &= \mathcal{F}_m\mathbf{x}_m + H_m(\mathbf{x}_{s'}, \mathbf{x}_m, h(\mathbf{x}_{s'}, \mathbf{x}_m, u), u)\\
\mathbf{x}_m(0) &= \mathbf{x}_{m0}\\
\mathbf{y}_c &= \mathcal{G}[\mathbf{x}_{s'}, \mathbf{x}_m, h(\mathbf{x}_{s'}, \mathbf{x}_m, u)]^T\\
\mathbf{y}_m &= \mathcal{Q}[\mathbf{x}_{s'}, \mathbf{x}_m, h(\mathbf{x}_{s'}, \mathbf{x}_m, u)]^T
\end{aligned} \tag{34}$$

where the state functions $\mathbf{x}_{s'} := [C_{s,s}, Q_{\text{sr}}, R_f]^T$ and $\mathbf{x}_m := [C_{s,m}, C_e, T]^T$. Given the solid-phase Li-ion concentration C_s simultaneously participates in normal diffusion and SEI film growth, it becomes two states after decomposition, i.e., $C_{s,m}$ and $C_{s,s}$. The functions $H_{s'}$ and H_m are continuous and bounded in their arguments for $(\mathbf{x}_{s'}, \mathbf{x}_m, u) \in \mathscr{H}_{s'} \times \mathscr{H}_m \times \mathbb{U}$ and $\mathscr{H}_{s'}, \mathscr{H}_m \subset \mathscr{H}$.

Assumption 4: The parameter ϵ_2 involved in battery SOH dynamic characteristics satisfies $\epsilon_2 \ll 1$.

Justification for Assumption 4: This can be readily justified using typical Li-ion batteries. During charge and discharge processes, the electrochemical and thermal states in a battery cell have significant change within a couple of minutes or hours. By comparison, the degree of battery degradation parameterized by ϵ_2 is several orders of magnitude slower than the normal intercalation reaction. Thus, in the timescale measured by the normal intercalation reaction, the parameter ϵ_2 as well as the change of battery SOH is negligibly small.

The battery system of Σ_s^2 has been identified to exhibit in the medium and slow timescales corresponding to the electrochemical, thermal, and aging phenomena. The smallness of ϵ_2 permits the SOH to work as a small perturbation for the normal intercalation reaction. According to Assumption 4, ϵ_2 is assumed to be 0, and as a result, the battery system (28) is simplified to the following boundary layer system with respect to the medium timescale state $\mathbf{x}_m$:

$$\begin{aligned}
\Sigma_m^3 : \dot{\mathbf{x}}_{s'} &= 0, \quad \mathbf{x}_{s'}(0) = \mathbf{x}_{s'0}\\
\dot{\mathbf{x}}_m &= \mathcal{F}_m\mathbf{x}_m + H_m(\mathbf{x}_{s'}, \mathbf{x}_m, h(\mathbf{x}_{s'}, \mathbf{x}_m, u), u)\\
\mathbf{x}_m(0) &= \mathbf{x}_{m0}\\
\mathbf{y}_c &= \mathcal{G}[\mathbf{x}_{s'}, \mathbf{x}_m, h(\mathbf{x}_{s'}, \mathbf{x}_m, u)]^T\\
\mathbf{y}_m &= \mathcal{Q}[\mathbf{x}_{s'}, \mathbf{x}_m, h(\mathbf{x}_{s'}, \mathbf{x}_m, u)]^T.
\end{aligned} \tag{35}$$

In the battery system (35), the differential equation in terms of $\mathbf{x}_{s'}$ from (34) is approximated by an algebraic equation through which the slow timescale state $\mathbf{x}_{s'}$ is fixed to be a constant, i.e., $\mathbf{x}_{s'0}$. After elimination of the dynamics of $\mathbf{x}_{s'}$, the state $\mathbf{x}_m$ is decoupled from the full-order battery system.

To individually investigate the behavior of the slow state $\mathbf{x}_{s'}$ that is governed by (34), further model simplification is needed as the medium and slow timescales are still simultaneously involved leading to undesirable computational complexity. In the usual practice of singular perturbation approaches, the slow system is derived by approximating the fast dynamics with their quasi-steady state values. However, the dynamics in the medium timescale do not approach a constant steady state, and this requires an alternative approach to analyze them.

From Assumption 2 and its justification, the system input $u(t)$ is known to the behavior in the medium timescale, which is the same as the state $\mathbf{x}_m$ does. Consideration of this and the smallness of ϵ_2 imposed by Assumption 4 motivates us to use averaging theory of [24] and [32] to simplify the process of deriving the slow battery model with the state $\mathbf{x}_{s'}$.

With this in mind, the solution of $\mathbf{x}_{s'}$ in the battery model (34) is considered to obtain by averaging the steady-state behavior of the medium battery system (35). Define a static average mapping $\mathbf{x}_{s'}(t) \to \mathcal{H}_{\text{av}}(\mathbf{x}_{s'}(t))$ as

$$\begin{aligned}
\mathcal{H}_{\text{av}}(\mathbf{x}_{s'}) := \lim_{T_s\to\infty} \frac{1}{T_s}\int_0^{T_s} &\mathcal{F}_m\mathbf{x}_m^*\\
&+ H_m\left(\mathbf{x}_{s'0}, \mathbf{x}_m^*, h\left(\mathbf{x}_{s'0}, \mathbf{x}_m^*, u^*\right), u^*\right)dt
\end{aligned} \tag{36}$$

where $u^*(t)$ is the specified system input and $\mathbf{x}_m^*(t)$ is the solution of the battery model (35) under the specified system input $u^*(t)$. In this *general average* mapping, it is worth mentioning that $\mathcal{H}_{\text{av}}$ is independent of ϵ_2 and $(\mathbf{x}_m(0), u(0)) \in \mathscr{H}_m \times \mathbb{U}/\{0\}$.

Therefore, in the slow timescale $\sigma = \epsilon_2 t$, the dynamics of $\mathbf{x}_{s'}$ from (34) is approximated by the following slow (average) battery system:

$$\Sigma_s^3 : \frac{d\mathbf{x}_{s'}}{d\sigma} = \mathcal{H}_{\text{av}}(\mathbf{x}_{s'}), \quad \mathbf{x}_{s'}(0) = \mathbf{x}_{s'0} \tag{37}$$
$$\mathbf{y}_c = \mathcal{G}\left[\mathbf{x}_{s'}, \mathbf{x}_m^*, h\left(\mathbf{x}_{s'}, \mathbf{x}_m^*, u^*\right)\right]^T. \tag{38}$$

To enable the above utilization of averaging theory in battery model simplification, an assumption is posed on the medium

timescale dynamics. Define a manifold $\bar{\mathbf{x}}_m = h'(\mathbf{x}_{s'0}, u)$ presenting the quasi-steady state of the medium state variables $\mathbf{x}_m$ from battery system of (35). Then $\bar{\mathbf{x}}_m$ is the solution of

$$\dot{\bar{\mathbf{x}}}_m(t) = \mathcal{F}_m \bar{\mathbf{x}}_m(t) + H_m(\bar{\mathbf{x}}_m(t), u(t)) \tag{39}$$

where $u(t) = u(t + kT_c)$, $\forall k = 0, 1 \ldots N$.

Assumption 5: There exists an integral manifold $\mathbf{z}_m := \mathbf{x}_m - \bar{\mathbf{x}}_m$, where $\bar{\mathbf{x}}_m$ is defined in (39), and a class-$\mathcal{KL}$ function β_h such that, for all initial conditions in the domain $\mathcal{D}$, the solutions of $\mathbf{x}_m$ in Σ_m^3 exist and satisfy

$$|\mathbf{z}_m| \leq \beta_h(|\mathbf{z}_m(0)|, t) \quad \forall t \geq 0. \tag{40}$$

Justification for Assumption 5: It is quantitatively investigated via simulations in Section V.

The state of $\mathbf{x}_{s'}$ has been decoupled from the original highly nonlinear battery system. To solve the developed mapping $\mathbf{x}_{s'} \rightarrow \mathcal{H}_{\text{av}}(\mathbf{x}_{s'})$, only the behavior of $\mathbf{x}_m$ governed by the battery system Σ_m^3 is required. Once such a mapping $\mathcal{H}_{\text{av}}$ is obtained, the slow battery system becomes very straightforward from (37) and (38).

Remark 4: To investigate battery SOH characteristics through the slow battery system, the input current $u(t)$ needs to be provided in advance. For any given profile of $u^*(t)$ including periodically or nonperiodically time-varying input current, there is a corresponding mapping defined by (36) and averaging theory can be used to simplify the battery model.

D. Application to Battery Models: Stage II

By applying the theoretical results in Section IV-C to the Li-ion battery system, the corresponding medium timescale battery model Σ_m^3 is provided in complete detail as

$$\begin{aligned}
\frac{\partial C_{s,m}^+(x,r,t)}{\partial t} &= \frac{D_s^{\text{eff},+}}{r^2}\frac{\partial}{\partial r}\left(r^2\frac{\partial C_{s,m}^+(x,r,t)}{\partial r}\right)\\
\frac{\partial C_s^-(x,r,t)}{\partial t} &= \frac{D_s^{\text{eff},-}}{r^2}\frac{\partial}{\partial r}\left(r^2\frac{\partial C_s^-(x,r,t)}{\partial r}\right)\\
\frac{\partial C_e^j(x,t)}{\partial t} &= \frac{\partial}{\partial x}\left(\frac{D_e^{\text{eff},j}}{\mu_e^j}\frac{\partial C_e^j(x,t)}{\partial x}\right) + \frac{\gamma^j}{F\mu_e^j}\frac{\partial i_e^j}{\partial x}\\
\rho^j c^j \frac{\partial T^j(x,t)}{\partial t} &= \lambda^j \frac{\partial^2 T^j(x,t)}{\partial x^2} - \left(I(t) - i_e^j(x,t)\right)\frac{\partial \Phi_s^j(x,t)}{\partial x}\\
&\quad - i_e^j(x,t)\frac{\partial \Phi_e^j(x,t)}{\partial x} + Fa^j J_I^j(x,t)\eta^j(x,t)\\
&\quad + Fa^j J_I^j(x,t)T^j(x,t)\Delta_S^j
\end{aligned}$$

where $J_I^{\pm}(x,t)$, $i_0^{\pm}(x,t)$, and $\eta^{\pm}(x,t)$ are formulated by the following algebraic equations:

$$\begin{aligned}
J_I^{\pm}(x,t) &= \frac{i_0^{\pm}(x,t)}{F}\left(e^{\frac{\alpha_n F\eta^{\pm}(x,t)}{RT^{\pm}(x,t)}} - e^{-\frac{\alpha_p F\eta^{\pm}(x,t)}{RT^{\pm}(x,t)}}\right)\\
i_0^{\pm}(x,t) &= k^{\pm}C_e(x,t)^{\alpha_n}\left(C_{\text{smax}}^{\pm} - C_{ss,m}^{\pm}(x,t)\right)^{\alpha_n} C_{ss,m}^{\pm}(x,t)^{\alpha_p}\\
\eta^{\pm}(x,t) &= \Phi_s^{\pm}(x,t) - \Phi_e^{\pm}(x,t) - U^{\pm}\left(C_{\text{ss}}^{\pm}(x,t)\right)\\
&\quad - FR_f(x,t_0)J_I^{\pm}(x,t).
\end{aligned}$$

In this battery model, the electrochemical–thermal dynamics are described, while the slow state variables, namely, $C_{s,s}$, Q_{sr}, and R_f, are all constant.

After sequential elimination of the electrical, electrochemical, and thermal dynamics, the slow battery model Σ_s^3 describing the battery aging behavior has been obtained in (37) and its dynamical equations in the corresponding Euclidian space are provided as

$$\begin{aligned}
\frac{\partial Q_{\text{sr}}(x,t)}{\partial t} &= \epsilon_2 a^- A^- L^- \lim_{T_s\to\infty}\frac{1}{T_s}\int_0^{T_s} e^{\phi(x,t)}dt\\
\frac{\partial R_f(x,t)}{\partial t} &= \epsilon_2\frac{M_f}{F\rho_f\sigma_f}\lim_{T_s\to\infty}\frac{1}{T_s}\int_0^{T_s} e^{\phi(x,t)}dt\\
\frac{\partial C_{s,s}(x,r,t)}{\partial t} &= \frac{\epsilon_2 a^- A^- L^-}{Q_{\max}T_s}\lim_{T_s\to\infty}\int_0^{T_s} C_{s,m}^*(x,r,t)e^{\phi(x,t)}dt\\
&\quad + \frac{D_s^{\text{eff},+}}{r^2 Q_{\max}T_s}\lim_{T_s\to\infty}\int_0^{T_s} Q_{\text{sr}}(x,t_0)\frac{\partial}{\partial r}\\
&\quad \times\left(r^2\frac{\partial C_{s,m}^*(x,r,t)}{\partial r}\right)dt
\end{aligned}$$

where the function $\phi(x,t)$ has the form of

$$\phi(x,t) = \frac{-\alpha_{\text{sr}}F\eta^*(x,t)}{RT^*(x,t)}$$

and the overpotential $\eta^*(x,t)$ is governed by

$$\eta^*(x,t) = \Phi_s^*(x,t) - \Phi_e^*(x,t) - U_{\text{sr}} - FR_f(x,t_0)J_I^*(x,t).$$

So far, the electrical, electrochemical, thermal, and aging dynamics within the battery states have been separated with families of simplified models obtained. The applied Assumptions 1–5 are similar to the timescale separation procedure of the singular perturbation approach and averaging theory in [24] and [32]. Given there is no formal tool to rigorously justify this model simplification framework, numerical solutions will be presented in the next section to validate these simplified models and their associated assumptions.

V. Validation via Simulations

The approximating properties of the simplified models Σ_f^2, Σ_m^3, and Σ_s^3 in comparison with those of the full-order model as well as their underlying assumptions are examined in this section through comprehensive simulations.

All the simulations are implemented in Modelica. To validate the established model simplification framework, different Li-ion cell chemistries can be used. Typical battery parameters listed in Table II are adopted from [15], [28], [33], and [34] and employed in this work. These parameters are related to a cylindrical $LiCoO_2/LiC_6$ battery cell with a 1.8-Ah nominal capacity.

The constant-current constant-voltage (CCCV) protocol is commonly used in current battery management systems and is considered here for battery model simulation. In this method, batteries are charged with an initial constant current for a period until its terminal voltage reaches a predefined threshold, and then the terminal voltage remains at its maximum value until the current drops below a given threshold. The design parameters in CCCV charging including initial current and current/voltage thresholds are, respectively, set up as 1.5C, 4.2 V, and 360 mA. C is a normalized metric indicating the input current utilized for operations in amperes relative to the

TABLE II
PARAMETERS OF LI-ION BATTERY USED IN THE SIMULATION

Symbol	Unit	Anode	Separator	Cathode
brug	–	4	4	4
$C_{s\max}$	mol/m^3	30555	–	50555
C_{s0}	mol/m^3	917	–	48977
C_{e0}	mol/m^3	1000	1000	1000
c	J/K·kg	1750.3	1329.3	2041.6
D_s	m^2/s	3.9×10^{-14}	–	1.0×10^{-14}
D_e	m^2/s	7.5×10^{-10}	7.5×10^{-10}	7.5×10^{-10}
h	W/(K·m^2)	5	–	5
i_{0sr}	A/m^2	1.5×10^{-6}	–	–
L	μm	88	20	80
k	Am$^{2.5}$/mol$^{1.5}$	4.854×10^{-6}	–	2.252×10^{-6}
R_p	μm	2	–	2
T_0	K	298	298	298
U_{sr}	V	0.4	–	–
α	–	0.5	–	0.5
α_{sr}	–	0.5	–	0.5
Δ_S	J/mol·K	0	0	0
γ	–	0.637	0.637	0.637
λ	W/K·m	0.809	1.172	0.553
ρ	kg/m^3	1233.3	1108.7	1356.7
σ	S/m	100	–	100
ε_s	–	0.49	–	0.59
ε_e	–	0.485	1	0.385
A	m^2	0.0596	0.0596	0.0596
F	C/mol		96487	
R	J/mol· k		8.314	

battery maximum rated capacity in ampere-hours. As such, 1C implies that a battery can be fully charged/discharged in 1 h. This set of parameters represents one of the fastest charging speeds as well as the crucial operating conditions utilized for most applications in the market including electric vehicles. Following the charging operation, a small constant current of 0.5C is applied for discharging with 3.2 V as the terminal condition.

Other charging schemes like the constant-current (CC) in different C-rates, multistage CC (MCC) [35], and the Urban Dynamometer Driving Schedule (UDDS) charging are also employed and these may warrant higher operating C-rates. To test the model fidelity at high C-rates, the initial UDDS data in [36] are augmented by a factor of three through which the maximum charging rate has been pushed to 3C. For CC charging, 1C, 2C, 3C, and 5C are, respectively, considered.

To demonstrate multiple battery charging and discharging cycles through methods of simulation, an assumption regarding the input currents is applied.

Assumption 6: The input current $u(t)$ for battery system is known *a priori* and is periodically time varying at different operating cycles.

Remark 5: The validity of Assumption 6 is tightly related to the practical utilization of a Li-ion battery. The charging process at each operating cycle can be controlled with its strategies predetermined in battery chargers. This makes it plausible to assume that the system input $u(t)$ is identical for battery charging at different cycles. For discharging cases, typical battery-powered devices are generally repeatedly used for similar tasks like UDDS for electric vehicles. Therefore, this is a good assumption for the purpose of simplifying the simulation process.

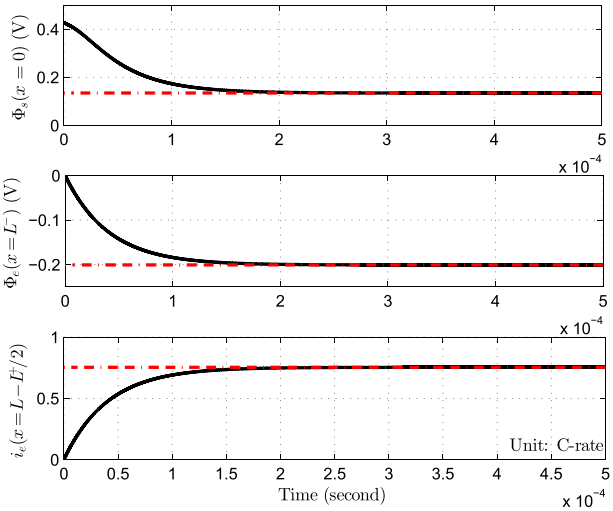

Fig. 4. Investigation of trajectories of the fast states Φ_s, Φ_e, and i_e via the fast battery model Σ_f^2 (black solid lines) and the quasi-steady state model (red dashed lines) in (27).

The integrator DASSL associated with Newton's method is used at each time step. Flexible integration stepsize and 0.0001 integration tolerance are chosen for these simulations. The spatial discretization method detailed in [37] is adopted in solving the PDE system with each electrode and separator discretized into 15 elements. The estimate error in SOC, SOH, or state variables is defined in the following form:

$$\beta(t) := (\omega_r(t) - \omega(t))/\omega_{\max}$$

where $\omega_r(t)$ and $\omega(t)$ represent solutions from the simplified models and the benchmark model, respectively, and $\omega_{\max}$ is the maximum value of $\omega(t)$.

A. Justification for Assumption 3

To justify Assumption 3 as well as to study trajectories of the fast state variables $\mathbf{x}_f$, the battery model Σ_f^2 is employed. In the fast timescale τ, the sampling time is chosen as 1e^{-8} s, which ensures that the maximum error in state prediction introduced by temporal discretization is within 0.01%. Based on the theoretical results in (27)–(33), simulations are implemented where the battery is charged in 1.5C within the considered time interval, and the results are shown in Fig. 4.

It can be clearly seen that the dynamics of the fast states Φ_s, Φ_e, and i_e all decay very quickly (within 0.0002 s). These states exponentially converge to their steady states in the corresponding timescale. The obtained results illustrate the existence of different timescales within the battery internal states and also qualitatively justify Assumption 3.

B. Justification for Assumption 5

To verify Assumption 5 and study the characteristics of the state variables $\mathbf{x}_m$ individually, simulations are implemented using the battery system of (35) and its quasi-steady state governed by (39).

The sampling time in studying the medium states corresponding to Li-ion diffusion dynamics is chosen as 1 s, which also ensures that the maximum error in state prediction

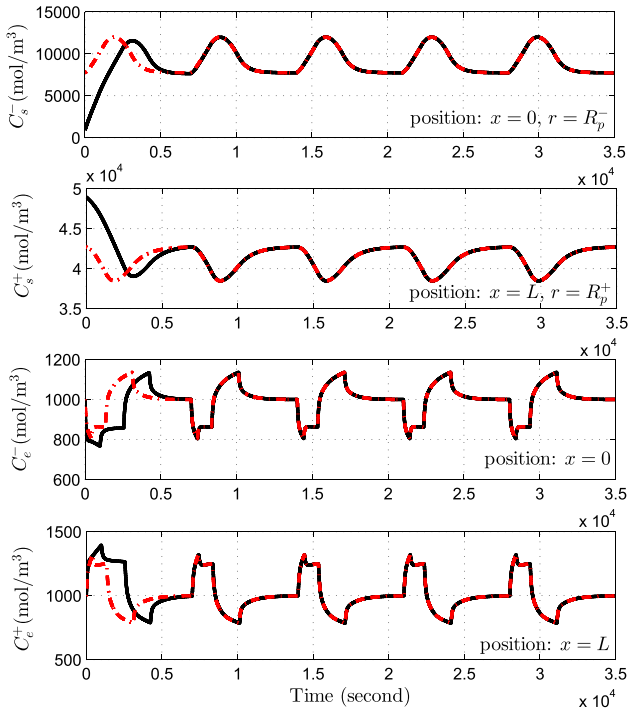

Fig. 5. Investigation of trajectories of the medium timescale states $\mathbf{x}_m$ using the battery model Σ_m^3 (black solid lines) and its quasi-steady state $\bar{\mathbf{x}}_m$ (red dashed lines) defined in (39).

introduced by temporal discretization is within 0.01%. To investigate the trajectories of $\mathbf{x}_m$ from the model Σ_m^3 and its quasi-steady state, different thresholds of the terminal voltage during operations can be chosen. Fig. 5 provides the simulation results regarding to the states, $C_s^{\pm}$ and $C_e^{\pm}$, for five operating cycles with 4 and 3.6 V as the voltage limits.

The medium state variables are shown to almost periodically vary in the course of battery operations. Although large deviations between $\mathbf{x}_m$ and $\bar{\mathbf{x}}_m$ are detected in the beginning, $\mathbf{x}_m - \bar{\mathbf{x}}_m$ is asymptotically reducing and approaching zero at about 7000 s. This result echoes our previous analysis on the medium timescale states used in the justification of Assumptions 1 and 4. Further observation finds that these states converge to their quasi-steady states, which are presented as periodically time-varying curves. Therefore, Assumption 5 that underpins the simplified models, Σ_f^3 and Σ_s^3, is plausible.

C. Justification for the Simplified Models

So far, all the assumptions behind the proposed model simplification framework have been justified. In the following, the closeness of solutions of the simplified models and the original model is examined. Given the fast electrical dynamics exhibit in microseconds, the full battery model that includes all the dynamics is involved in numerical stiffness issue and is impractical to simulate. In view of this, to study the behaviors of $\mathbf{x}_m$ and $\mathbf{x}_s$, the model Σ_s^2 that well approximates the original model in the slow and medium timescales is used as a test bed. The sampling time in this process is chosen as 1 s, in the similar way as in Section V-B.

To examine the model fidelity under the specified CCCV, a CC or an UDDS charging strategy, the following evaluation procedure using the averaged system Σ_s^3 and the simplified

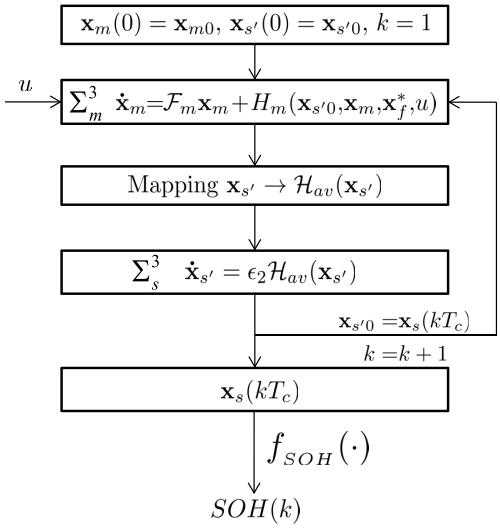

Fig. 6. Procedure for battery charging strategy evaluation using the simplified models Σ_m^3 and Σ_s^3.

model Σ_m^3 from the established framework is proposed. Here, degradation to 80% of the initial SOH is used to quantify the battery's lifetime.

Procedure 1:

1) Specify initial conditions of the states $[\mathbf{x}_{s'0}, \mathbf{x}_{m0}]$ and the cycle number $k = 1$.
2) Run the battery model (35) under the specified charging strategy.
3) Calculate the static mapping $\mathbf{x}_{s'} \to \mathcal{H}_{\text{av}}(\mathbf{x}_{s'})$ using (36). For arbitrary initial conditions, a sufficiently large value of T_s can be chosen to approach the infinite time interval. If the initial values $\mathbf{x}_{s0}$ and $\mathbf{x}_{m0}$ are within the limit cycles of the steady state of the $\mathbf{x}_m$, then in practice, T_s can be set to T_c.
4) Run the averaged battery system (37)–(38) and record $\mathbf{x}_{s'}$ at the time $t = kT_c$.
5) Calculate SOH using (19).
6) If SOH $> 80\%$, then increment k, update $\mathbf{x}_{s'0}$ and go to Step 2, or else go to Step 7.
7) Output the battery lifetime SOH(k).

To further illustrate the implementation of the simplified models Σ_m^3 and Σ_s^3 in Procedure 1 for the investigation of battery SOH characteristics, a flowchart depicting this sequence is provided in Fig. 6.

Fig. 7 shows the simulation results under the CCCV charging. It can be seen that good agreement between the model Σ_m^3 and the benchmark Σ_s^2 is obtained for all the medium timescale states including $C_s^{\pm}, C_e^{\pm}$, and $T^{\pm,\text{sep}}$. The electrolyte concentrations whose dynamics are often ignored at low charging rates [7] are studied. Here, it is demonstrated that their changes in both the negative and positive electrodes are as large as 70% and are thus not negligible under the applied charging conditions. Indeed, the developed simplified model Σ_m^3 accurately captures the electrolyte concentration characteristics. The approximation error in SOC prediction is seen to be less than 0.2%. Further examination of this model under UDDS and CC charging protocols is given in Figs. 8 and 9(a), where small errors are again observed.

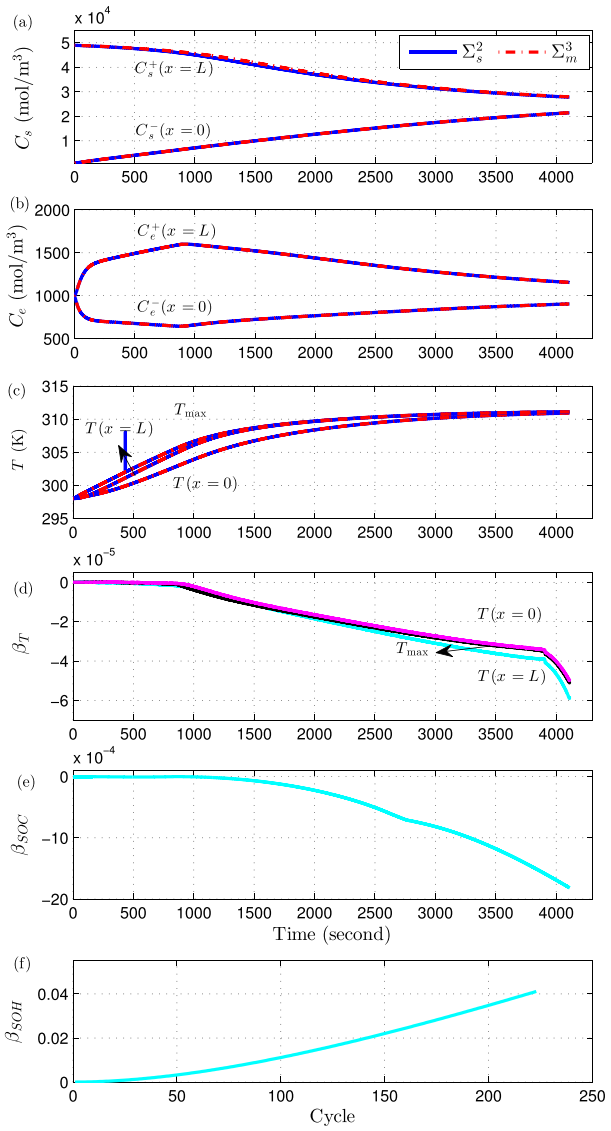

Fig. 7. Validation of the simplified battery models Σ_m^3 and Σ_s^3 under the CCCV charging test. (a) Solid-phase Li-ion concentration. (b) Electrolyte concentration. (c) Temperature. (d) Temperature error. (e) SOC error. (f) SOH error.

At this scale of modeling error and over the time intervals of the driving cycles, the derived medium timescale model Σ_m^3 is able to capture the electrochemical–thermal dynamics well.

In some circumstances, such as limited operating range of the cell, further model reductions may be possible. For example, with additional assumptions of constant temperature and/or electrolyte concentration (as might be observed from low charge/discharge rates), the model Σ_m^3 degenerates into the single particle model (SPM) with two lumped states in the battery system or SPM with additional electrolyte states, as used in [37]–[40].

The percentage error in SOH prediction under the CCCV charging approach is plotted in Fig. 7(f). For automotive applications, 20% capacity loss from the initial maximum capacity is often considered as the end of battery's life (EOL), which corresponds to 223 operating cycles in this case. Although it becomes larger with the increased cycles, the modeling error in SOH at EOL is less than 5%. Such a

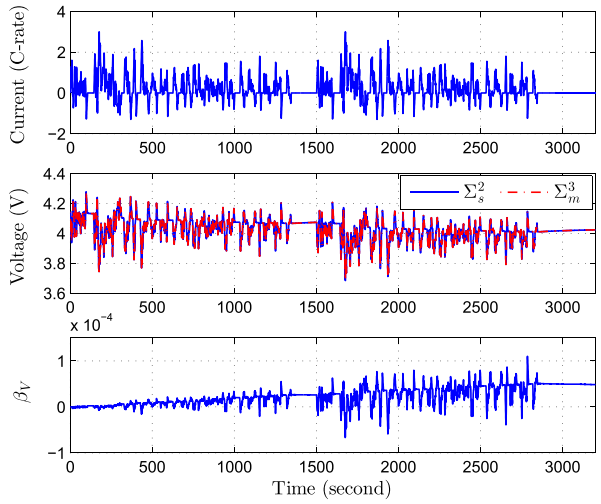

Fig. 8. Validation of the battery model Σ_m^3 under two concatenated UDDS tests.

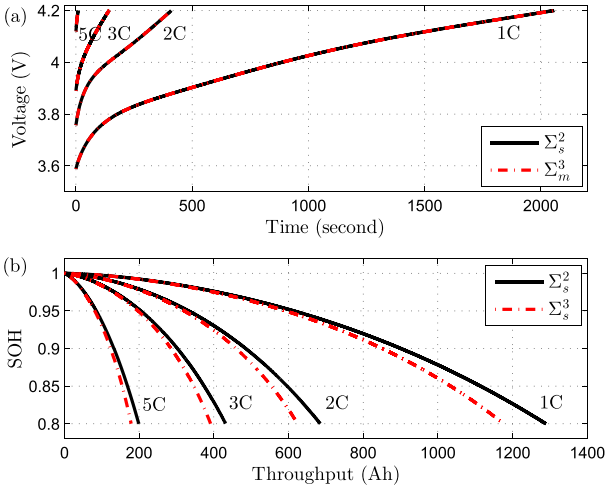

Fig. 9. Validation of Σ_m^3 and Σ_s^3 under the 1C, 2C, 3C, and 5C C-rate CC charging schemes. (a) Battery is charged to 4.2 V. (b) Battery is charged with a 10% SOC increase and then discharged under 0.5C to 3.2 V in each cycle.

small magnitude of error tells that the SOH dynamics can be well approximated by the developed slow model Σ_s^3. Further validations of this model under CC charging in different C-rates are given in Fig. 9(b). These show that the model Σ_s^3 is able to follow the higher order model Σ_s^2 over a range of operating rates including the case of 5C. In addition, the aging indicated by the simplified model is slightly faster than Σ_s^2. This is not as concerning as the alternative, as it will likely lead to algorithms that protect batteries when the simplified model is used in model-based optimization and control applications.

VI. Application for Charging Strategy Evaluation

With the theoretical result with regard to the battery model simplification framework, we are now in the position to put it into practice. The simplified models Σ_m^3 and Σ_s^3 have various applications including the following:

1) assessment on the effects of different charging strategies by means of simulation instead of the original model or experiments;

2) model-based estimation, control, and optimization for battery dynamic performance and lifetime.

An example given in the following demonstrates the analysis capability of the proposed framework for charging strategy evaluation.

An MCC charging strategy was shown to have significant improvement relative to the CCCV charging method in the SOH and required charging time through a large number of experiments in [35] and [41]. Based on this charging method and a boost charging algorithm of [42], an alternative MCC charging strategy is proposed for the purpose of comparison. While the proposed strategy is *ad hoc* in terms of the determination of C-rate, voltage limit, and duration during each stage, it is useful to demonstrate the potential differences in battery states that may be observed from the simplified models.

The simulation environment and setup being used are the same as in Section V. To ensure that the temporal discretization error is within 0.01%, the sampling time is chosen as 1 and 1000 s separately for the medium and slow timescale states. All the simulations are conducted on a desktop computer with a 3.4-GHz processor and an 8-GB RAM. The CPU time for integration is recorded for the assessment of computational efficiency.

Using Procedure 1, simulations of the CCCV, MCC, and the proposed method are implemented with the results provided in Fig. 10. It is found the MCC is able to support 60% more life cycles and save 17.6% charging times relative to the CCCV. Another way to test the proposed model simplification framework is to implement it in experiments. It is worthy mentioning that the simulation results with regard to the advantages of the MCC method compared with the CCCV are consistent with the experimental outputs observed from [35]. Meanwhile, the proposed charging method can transfer similar capacity to the battery, but achieves 13% more lifetime and 11.6% less charging times compared with the MCC. This may be useful information for developing optimal charging strategies.

These three charging strategies have been compared using simplified battery models from the proposed modeling framework. Here, it is important for the reader to note that the developed procedure for charging strategy evaluation is sufficiently general as to be equally applicable to other charging strategies.

In addition, battery characteristics can be analyzed based on the simulation results of Fig. 10. From the static map $Q \rightarrow \mathcal{H}_{\text{av}}(Q)$, the aging rate is found to slow down gradually with the decreased available capacity. This is potentially because the passive SEI film gets thicker with battery degradation and suppresses further active Li-ion corrosion and reductive electrolyte decomposition.

The benefit of using simplified battery models for charging strategy assessment rather than the full-order battery model and experimental approaches would be the reduced computational effort. To show this, Table III compares the computational times for simulating 400 cycles associated with different battery models. It can be seen that with model simplification proceeded, the required times are greatly decreased. Using Σ_m^3 and Σ_s^3 as proposed in Procedure 1 rather than the high-order model Σ_s^2, the time of 29.8% can be saved. While for the calculation of electrochemical–thermal dynamics, the model Σ_m^3 is able to offer 38.6% computational time saving. For SOH prediction, if the static mapping as shown in Fig. 10(c) is available *a priori*, simulations using Σ_s^3 become extremely fast. Thus, this proposed evaluation system based on simplified models is able to significantly expedite the analysis of different charging strategies.

The accuracy of these simplified models has been validated in the previous section against the initial battery model. Indeed, the accuracy of charging strategy evaluation greatly depends on the fidelity of the initial model.

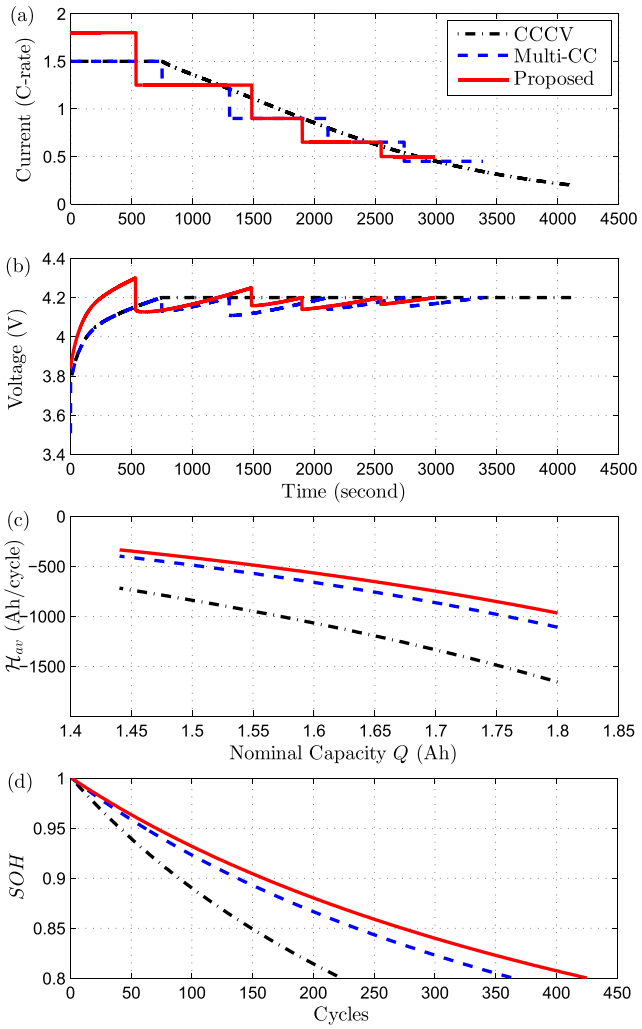

Fig. 10. Comparisons of the CCCV, MCC charging [35], and proposed charging method. (a) Input current profiles. (b) Terminal voltage profiles. (c) Static mapping from spatially averaged Q to $\mathcal{H}_{\text{av}}(Q)$. (d) Variations of SOH with cycling.

TABLE III

COMPARISON OF COMPUTATIONAL TIMES ASSOCIATED WITH DIFFERENT BATTERY MODELS

Models	Sampling time (s)	Simulation time (mins) for 400 cycles
Σ_s^2	1	171
$\Sigma_s^3 + \Sigma_m^3$	1	120
Σ_m^3	1	105
Σ_s^3	1000	1.8×10^{-4}

Factors contributing to battery degradation are various and complex [18]. Although a dominant aging mechanism, namely, SEI film-based aging, has been considered in this model, the identification and quantification of other aging mechanisms are still an ongoing work. It is worth noting that the methodology developed in the work for PDE battery model simplification is general.

VII. Conclusion

In this paper, a physics-based model for Li-ion battery that accurately captures the electrochemical, thermal, electrical, and aging dynamics has been proposed. Starting from this initial system formulation, a novel framework for PDE battery model simplification was developed by judicious use of a singular perturbation approach and averaging theory. The novelty arises from the systematic simplification procedure through which the underlying assumptions imposed on simplified models can be explicitly stated.

Through comprehensive simulations, the simplified models have been observed to be capable of efficiently predicting battery dynamic characteristics. The developed model simplification framework including families of battery models is sufficiently general covering different battery types and a range of applications.

To demonstrate the analysis capability of this framework, a model-based evaluation procedure for battery charging strategies was proposed. This procedure, synthesized from the simplified models, rather than other higher order model was illustrated as a useful tool for quickly and accurately evaluating different charging strategies. The development of more complete aging models can be integrated into the initial battery model to achieve higher accuracy for SOH prediction.

Opportunities for future work include analytical justification of Assumptions 3 and 5, which were shown to hold using numerical methods here. Furthermore, there are opportunities to apply the simplified models in the design of multiple timescale observers for battery SOC and SOH. Similarly, potential research gaps exist in optimization and controller design for battery fast charging using simplified electrochemistry-based models.

Appendix

The matrix functions and parameters involved in battery model reformulation of Section III are explicitly provided in the following.

In (20), F_1, F_2, S_1, S_2, and H are all matrix functions and can be decomposed into

$$\begin{aligned} F_1 &= \operatorname{diag}\big(F_1^-, F_1^{\text{sep}}, F_1^+\big), \quad F_2 = \operatorname{diag}\big(F_2^-, F_2^{\text{sep}}, F_2^+\big) \\ S_1 &= \operatorname{diag}\big(S_1^-, S_1^{\text{sep}}, S_1^+\big), \quad S_2 = \operatorname{diag}\big(S_2^-, S_2^{\text{sep}}, S_2^+\big) \\ H &= \operatorname{diag}(H^-, H^{\text{sep}}, H^+). \end{aligned}$$

In these matrices, the vector functions can be derived from the battery dynamic equations (4)–(16) and are further explicitly provided as

$$\begin{aligned} F_1^- &= \operatorname{diag}\big(2D_s^{\text{eff},-}/r, 0, 0, 0, 0, 0, 0, 0\big) \\ F_1^+ &= \operatorname{diag}\big(2D_s^{\text{eff},+}(1 - Q_{\text{sr}}/Q_{\max}), 0, 0, 0, 0, 0\big) \\ F_2^- &= \operatorname{diag}\big(D_s^{\text{eff},-}, 0, 0, 0, 0, 0, 0\big) \\ F_2^+ &= \operatorname{diag}\big(D_s^{\text{eff},+}(1 - Q_{\text{sr}}/Q_{\max}), 0, 0, 0, 0, 0\big) \\ F_1^{\text{sep}} &= F_2^{\text{sep}} = \text{zeros}(3, 3) \\ S_2^- &= \operatorname{diag}\big(0, D_e^{\text{eff},-}/\mu_e^-, 0, 0, 0, \lambda^-/(\rho^- c^-), 0, 0\big) \\ S_2^+ &= \operatorname{diag}\big(0, D_e^{\text{eff},+}/\mu_e^+, 0, 0, 0, \lambda^+/(\rho^+ c^+)\big) \\ S_2^{\text{sep}} &= \operatorname{diag}\big(D_e^{\text{eff,sep}}/\mu_e^{\text{sep}}, 0, \lambda^{\text{sep}}/(\rho^{\text{sep}} c^{\text{sep}})\big) \end{aligned}$$

$$S_1^+ = \begin{pmatrix} 0 & 0 & 0 & 0 & 0 & 0 & 0 & 0 \\ 0 & 0 & 0 & 0 & \frac{\gamma^+}{F\mu_e^+} & 0 & 0 & 0 \\ 0 & 0 & \frac{1}{\epsilon_{\Phi s}} & 0 & 0 & 0 & 0 & 0 \\ 0 & \frac{-2R\gamma^+ T^+}{F\epsilon_{\Phi s} C_e^+} & 0 & \frac{1}{\epsilon_{\Phi e}} & 0 & 0 & 0 & 0 \\ 0 & 0 & 0 & 0 & \frac{1}{\epsilon_{ie}} & 0 & 0 & 0 \\ 0 & 0 & \frac{-I + i_e^+}{\rho^+ c^+} & \frac{-i_e^+}{\rho^+ c^+} & 0 & 0 & 0 & 0 \end{pmatrix}$$

$$H^+ = \begin{pmatrix} -Fa^- A^- L^- J_{\text{sr}} C_s^+ Q_{\max}^{-1} \\ 0 \\ \big(I - i_e^+\big)(\epsilon_{\Phi s}\sigma^{\text{eff},+})^{-1} \\ i_e^+ (\epsilon_{\Phi e}\kappa^{\text{eff},+})^{-1} \\ Fa^+ J^+ \epsilon_{ie}^{-1} \\ Fa^+ J^+ \big(\eta^+ + T^+ \Delta_S^+\big)(\rho^+ c^+)^{-1} \end{pmatrix}$$

$$S_1^{\text{sep}} = \begin{pmatrix} 0 & 0 & 0 \\ -\frac{2R\gamma^{\text{sep}} T^{\text{sep}}}{F C_e^{\text{sep}} \epsilon_{\Phi e}} & \frac{1}{\epsilon_{\Phi e}} & 0 \\ 0 & \frac{-I}{\rho^{\text{sep}} c^{\text{sep}}} & 0 \end{pmatrix}$$

$$H^{\text{sep}} = \begin{pmatrix} 0 & -\frac{i^{\text{sep}}}{\kappa^{\text{eff,sep}} \epsilon_{\Phi e}} & 0 \end{pmatrix}^T$$

$$S_1^- = \begin{pmatrix} 0 & 0 & 0 & 0 & 0 & 0 & 0 & 0 \\ 0 & 0 & 0 & 0 & \frac{\gamma^-}{F\mu_e^-} & 0 & 0 & 0 \\ 0 & 0 & \frac{1}{\epsilon_{\Phi s}} & 0 & 0 & 0 & 0 & 0 \\ 0 & \frac{-2R\gamma^- T^-}{F\epsilon_{\Phi s} C_e^-} & 0 & \frac{1}{\epsilon_{\Phi e}} & 0 & 0 & 0 & 0 \\ 0 & 0 & 0 & 0 & \frac{1}{\epsilon_{ie}} & 0 & 0 & 0 \\ 0 & 0 & \frac{-I + i_e^-}{\rho^- c^-} & \frac{-i_e^-}{\rho^- c^-} & 0 & 0 & 0 & 0 \\ 0 & 0 & 0 & 0 & 0 & 0 & 0 & 0 \\ 0 & 0 & 0 & 0 & 0 & 0 & 0 & 0 \end{pmatrix}$$

$$H^- = \begin{pmatrix} 0 \\ 0 \\ \big(I - i_e^-\big)(\epsilon_{\Phi s}\sigma^{\text{eff},-})^{-1} \\ i_e^- (\epsilon_{\Phi e}\kappa^{\text{eff},-})^{-1} \\ Fa^- J^- \epsilon_{ie}^{-1} \\ Fa^- J^- \big(\eta^- + T^- \Delta_S^-\big)(\rho^- c^-)^{-1} \\ -Fa^- A^- L^- J_{\text{sr}} \\ -M_f J_{\text{sr}} (\rho_f \sigma_f)^{-1} \end{pmatrix}.$$

In (23), the parameter matrices $C_1, \ldots, C_8$ and $D_1, \ldots, D_8$ are provided in the following:

$$
\begin{aligned}
C_1 &= \operatorname{diag}(0, \ldots, 0, 1, 0, 0, 0) \\
C_2 &= \operatorname{diag}(0, 1, 0, 0, 0, -\lambda^-, 0, 0) \\
C_3 &= \operatorname{diag}(0, \ldots, 0, 1, 0) \\
C_4 &= \operatorname{diag}(0, 1, 0, 0, 0, -\lambda^+) \\
C_5 &= C_7 = \operatorname{diag}(1, 0, \ldots, 0) \\
C_6 &= C_8 = \operatorname{diag}(1, 0, \ldots, 0) \\
D_1 &= [0, \ldots, 0, h \cdot (T_{\text{amb}} - T^-), 0, 0]^T \\
D_2 &= [0, \ldots, 0, h \cdot (-T_{\text{amb}} + T^+)]^T \\
D_3 &= \left[- J^-/D_s^{\text{eff},-}, 0, \ldots, 0 \right]^T \\
D_4 &= \left[- J^+/D_s^{\text{eff},+}, 0, \ldots, 0 \right]^T \\
D_5 &= D_7 = \operatorname{diag}(0, 1, 0, 1, 1, 1) \\
D_6 &= \operatorname{diag}\big(0, D_e^{\text{eff,sep}}/D_e^{\text{eff},-}, 0, 0, 0, \lambda^{\text{sep}}/\lambda^-\big) \\
D_8 &= \operatorname{diag}\big(0, D_e^{\text{eff},+}/D_e^{\text{eff,sep}}, 0, 0, 0, \lambda^+/\lambda^{\text{sep}}\big).
\end{aligned}
$$

REFERENCES

[1] M. Armand and J.-M. Tarascon, "Building better batteries," *Nature*, vol. 451, no. 7179, pp. 652–657, 2008.

[2] X. Hu, S. Li, and H. Peng, "A comparative study of equivalent circuit models for Li-ion batteries," *J. Power Sour.*, vol. 198, pp. 359–367, Jan. 2012.

[3] X. Hu, R. Xiong, and B. Egardt, "Model-based dynamic power assessment of lithium-ion batteries considering different operating conditions," *IEEE Trans. Ind. Informat.*, vol. 10, no. 3, pp. 1948–1959, Aug. 2014.

[4] F. Sun, X. Hu, Y. Zou, and S. Li, "Adaptive unscented Kalman filtering for state of charge estimation of a lithium-ion battery for electric vehicles," *Energy*, vol. 36, no. 5, pp. 3531–3540, 2011.

[5] M. Doyle, T. F. Fuller, and J. Newman, "Modeling of galvanostatic charge and discharge of the lithium/polymer/insertion cell," *J. Electrochem. Soc.*, vol. 140, no. 6, pp. 1526–1533, 1993.

[6] N. A. Chaturvedi, R. Klein, J. Christensen, J. Ahmed, and A. Kojic, "Algorithms for advanced battery-management systems," *IEEE Control Syst.*, vol. 30, no. 3, pp. 49–68, Jun. 2010.

[7] R. Klein, N. A. Chaturvedi, J. Christensen, J. Ahmed, R. Findeisen, and A. Kojic, "Electrochemical model based observer design for a lithium-ion battery," *IEEE Trans. Control Syst. Technol.*, vol. 21, no. 2, pp. 289–301, Mar. 2013.

[8] V. R. Subramanian, V. Boovaragavan, V. Ramadesigan, and M. Arabandi, "Mathematical model reformulation for lithium-ion battery simulations: Galvanostatic boundary conditions," *J. Electrochem. Soc.*, vol. 156, no. 4, pp. A260–A271, 2009.

[9] M. Corno, N. Bhatt, S. M. Savaresi, and M. Verhaegen, "Electrochemical model-based state of charge estimation for Li-ion cells," *IEEE Trans. Control Syst. Technol.*, vol. 23, no. 1, pp. 117–127, Jan. 2015.

[10] S. Anwar, C. Zou, and C. Manzie, "Distributed thermal-electrochemical modeling of a lithium-ion battery to study the effect of high charging rates," in *Proc. 19th IFAC World Congr.*, 2014, vol. 19. no. 1, pp. 6258–6263.

[11] W. B. Gu and C. Y. Wang, "Thermal-electrochemical modeling of battery systems," *J. Electrochem. Soc.*, vol. 147, no. 8, pp. 2910–2922, 2000.

[12] P. Ramadass, B. Haran, R. White, and B. N. Popov, "Mathematical modeling of the capacity fade of Li-ion cells," *J. Power Sour.*, vol. 123, no. 2, pp. 230–240, 2003.

[13] J. Wang *et al.*, "Cycle-life model for graphite-$LiFePO_4$ cells," *J. Power Sour.*, vol. 196, no. 8, pp. 3942–3948, 2011.

[14] S. B. Peterson, J. Apt, and J. F. Whitacre, "Lithium-ion battery cell degradation resulting from realistic vehicle and vehicle-to-grid utilization," *J. Power Sour.*, vol. 195, no. 8, pp. 2385–2392, 2010.

[15] P. Ramadass, B. Haran, P. M. Gomadam, R. White, and B. N. Popov, "Development of first principles capacity fade model for Li-ion cells," *J. Electrochem. Soc.*, vol. 151, no. 2, pp. A196–A203, 2004.

[16] G. Ning, R. E. White, and B. N. Popov, "A generalized cycle life model of rechargeable Li-ion batteries," *Electrochim. Acta*, vol. 51, no. 10, pp. 2012–2022, 2006.

[17] P. Liu *et al.*, "Aging mechanisms of $LiFePO_4$ batteries deduced by electrochemical and structural analyses," *J. Electrochem. Soc.*, vol. 157, no. 4, pp. A499–A507, 2010.

[18] A. Barré, B. Deguilhem, S. Grolleau, M. Gérard, F. Suard, and D. Riu, "A review on lithium-ion battery ageing mechanisms and estimations for automotive applications," *J. Power Sour.*, vol. 241, pp. 680–689, Nov. 2013.

[19] A. V. Randall, R. D. Perkins, X. Zhang, and G. L. Plett, "Controls oriented reduced order modeling of solid-electrolyte interphase layer growth," *J. Power Sour.*, vol. 209, pp. 282–288, Jul. 2012.

[20] S. J. Moura, J. L. Stein, and H. K. Fathy, "Battery-health conscious power management in plug-in hybrid electric vehicles via electrochemical modeling and stochastic control," *IEEE Trans. Control Syst. Technol.*, vol. 21, no. 3, pp. 679–694, May 2013.

[21] M. Muratori, M. Canova, Y. Guezennec, and G. Rizzoni, "A reduced-order model for the thermal dynamics of Li-ion battery cells," in *Proc. 6th IFAC Symp. Adv. Automotive Control*, Jul. 2010, pp. 192–197.

[22] C. Speltino, D. Di Domenico, G. Fiengo, and A. Stefanopoulou, "Comparison of reduced order lithium-ion battery models for control applications," in *Proc. IEEE 48th CDC*, Dec. 2009, pp. 3276–3281.

[23] J. C. Forman, S. Bashash, J. L. Stein, and H. K. Fathy, "Reduction of an electrochemistry-based Li-ion battery model via quasi-linearization and Padé approximation," *J. Electrochem. Soc.*, vol. 158, no. 2, pp. A93–A101, 2011.

[24] P. Kokotović, H. K. Khalil, and J. O'Reilly, *Singular Perturbation Methods in Control: Analysis and Design*, vol. 25. Philadelphia, PA, USA: SIAM, 1999.

[25] M. Premaratne, D. Nešić, and G. P. Agrawal, "Pulse amplification and gain recovery in semiconductor optical amplifiers: A systematic analytical approach," *J. Lightw. Technol.*, vol. 26, no. 12, 1653–1660, Jun. 15, 2008.

[26] P. D. Christofides, *Nonlinear and Robust Control of PDE Systems: Methods and Applications to Transport-Reaction Processes*. Boston, MA, USA: Springer Science & Business Media, 2012.

[27] J. T.-Y. Wen and M. J. Balas, "Robust adaptive control in Hilbert space," *J. Math. Anal. Appl.*, vol. 143, no. 1, pp. 1–26, 1989.

[28] M. Doyle, J. Newman, A. S. Gozdz, C. N. Schmutz, and J.-M. Tarascon, "Comparison of modeling predictions with experimental data from plastic lithium ion cells," *J. Electrochem. Soc.*, vol. 143, no. 6, pp. 1890–1903, 1996.

[29] J. Newman and K. E. Thomas-Alyea, *Electrochemical Systems*. New York, NY, USA: Wiley, 2012.

[30] C. P. Steinmetz and J. L. R. Hayden, *Steinmetz Electrical Engineering Library: Theory and calculation of Transient Electric Phenomena and Oscillations*, vol. 8. New York, NY, USA: McGraw-Hill, 1920.

[31] P. V. Kokotovic, R. O'Malley, Jr., and P. Sannuti, "Singular perturbations and order reduction in control theory—An overview," *Automatica*, vol. 12, no. 2, pp. 123–132, 1976.

[32] A. R. Teel, L. Moreau, and D. Nesic, "A unified framework for input-to-state stability in systems with two time scales," *IEEE Trans. Autom. Control*, vol. 48, no. 9, pp. 1526–1544, Sep. 2003.

[33] W.-B. Gu and C.-Y. Wang, "Thermal and electrochemical coupled modeling of a lithium-ion cell," *Proc. Electrochem. Soc.*, vol. 99, no. 1, pp. 748–762, 2000.

[34] S. C. Chen, C. C. Wan, and Y. Y. Wang, "Thermal analysis of lithium-ion batteries," *J. Power Sour.*, vol. 140, no. 1, pp. 111–124, 2005.

[35] Y.-H. Liu and Y.-F. Luo, "Search for an optimal rapid-charging pattern for Li-ion batteries using the Taguchi approach," *IEEE Trans. Ind. Electron.*, vol. 57, no. 12, pp. 3963–3971, Dec. 2010.

[36] C. Zou, A. G. Kallapur, C. Manzie, and D. Nešić, "PDE battery model simplification for SOC and SOH estimator design," in *Proc. 54th IEEE Conf. Decision Control*, 2015, pp. 1–6.

[37] C. Zou, C. Manzie, and S. Anwar, "Control-oriented modeling of a lithium-ion battery for fast charging," in *Proc. 9th IFAC World Congr.*, 2014, pp. 3912–3917.

[38] S. J. Moura, N. A. Chaturvedi, and M. Krstić, "Adaptive partial differential equation observer for battery state-of-charge/state-of-health estimation via an electrochemical model," *J. Dyn. Syst. Meas. Control*, vol. 136, no. 1, p. 011015, 2014.

[39] S. Tang, Y. Wang, Z. Sahinoglu, T. Wada, S. Hara, and M. Krstić, "State-of-charge estimation for lithium-ion batteries via a coupled thermal-electrochemical model," in *Proc. Amer. Control Conf.*, 2015, pp. 5871–5877.

[40] C. Manzie, C. Zou, and D. Nešić, "Simplification techniques for PDE-based Li-ion battery models," in *Proc. IEEE Conf. Decision Control*, Osaka, Japan, 2015, pp. 1–9.

[41] Y.-H. Liu, C.-H. Hsieh, and Y.-F. Luo, "Search for an optimal five-step charging pattern for Li-ion batteries using consecutive orthogonal arrays," *IEEE Trans. Energy Convers.*, vol. 26, no. 2, pp. 654–661, Jun. 2011.

[42] P. H. L. Notten, J. H. G. Op het Veld, and J. R. G. van Beek, "Boostcharging Li-ion batteries: A challenging new charging concept," *J. Power Sour.*, vol. 145, no. 1, pp. 89–94, 2005.

Changfu Zou (S'15) received the B.E. degree in automotive engineering from the Beijing Institute of Technology, Beijing, China, in 2011. He is currently pursuing the Ph.D. degree with the Department of Mechanical Engineering, The University of Melbourne, Melbourne, VIC, Australia, and NICTA Victoria, Melbourne.

His thesis investigates Li-ion battery model simplification and model-based applications, including charging strategy evaluation, observer design for state-of-charge and state-of-health estimation, and optimal fast charging control.

Mr. Zou was a recipient of the Excellent Graduate of Beijing.

Chris Manzie (SM'14) was a Visiting Scholar with the University of California at San Diego, San Diego, CA, USA, in 2007, and a Visiteur Scientifique with IFP Energies Nouvelles, Rueil-Malmaison, France, in 2012. He is currently a Professor with the Department of Mechanical Engineering, The University of Melbourne, Melbourne, VIC, Australia. He is also an Assistant Dean (Research Training) and the Mechatronics Discipline Coordinator with the Melbourne School of Engineering. His current research interests include model-based and model-free control and optimization, with applications in a range of areas, including systems related to energy, transportation, and mechatronics.

Prof. Manzie is a member of the IFAC Technical Committees on Automotive Control and the IFAC Technical Committee on Mechatronics. He received the Future Fellowship by the Australian Research Council from 2010 to 2014. He is an Associate Editor of *Control Engineering Practice* (Elsevier), the IEEE TRANSACTIONS ON MECHATRONICS/*ASME Transactions on Mechatronics*, and the *Australian Journal of Electrical and Electronic Engineering*.

Dragan Nešić (F'08) received the B.E. degree in mechanical engineering from the University of Belgrade, Belgrade, Serbia, in 1990, and the Ph.D. degree from Systems Engineering, RSISE, Australian National University, Canberra, ACT, Australia, in 1997.

He has been with The University of Melbourne, Melbourne, VIC, Australia, since 1999, where he is currently a Professor with the Department of Electrical and Electronic Engineering. His current research interests include networked control systems, discrete-time, sampled-data and continuous-time nonlinear control systems, input-to-state stability, extremum seeking control, applications of symbolic computation in control theory, and hybrid control systems.

Prof. Nešić is a fellow of the Institution of Engineers, Australia. He received the Humboldt Research Fellowship by the Alexander von Humboldt Foundation in 2003, an Australian Professorial Fellowship from 2004 to 2009, and the Future Fellowship by the Australian Research Council from 2010 to 2014. He has been a Distinguished Lecturer of the IEEE Control Systems Society since 2008. He served as an Associate Editor of *Automatica*, the IEEE TRANSACTIONS ON AUTOMATIC CONTROL, *Systems and Control Letters*, and the *European Journal of Control* journals.